Characterization of radiation damage in ceramics: Old challenge new issues?

David Simeone[a)]
CEA/DEN/DANS/DMN/SRMA/LA2M-LRC CARMEN, CEN Saclay, F91191 Gif sur Yvette, France; and SPMS/ECP UMR 8580/LRC CARMEN, Ecole Centrale Paris, F91292 Chatenay Malabry, France

Jean Marc Costantini
CEA/DEN/DANS/DMN/SRMA/LA2M, CEN Saclay, F91191 Gif sur Yvette, France

Laurence Luneville
CEA/DEN/DANS/DM2S/SERMA/LLPR-LRC CARMEN, CEN Saclay, F91191 Gif sur Yvette, France; and SPMS/ECP UMR 8580/LRC CARMEN, Ecole Centrale Paris, F91292 Chatenay Malabry, France

Lionel Desgranges
CEA/DEN/CAD/DEC/SESC/LLC, CEN Cadarache, F13108 Saint-Paul-Lez Durance, France

Patrick Trocellier
CEA/DEN, Service de Recheches de Métallurgie Physique, Laboratoire JANNUS, F-91191 Gif-sur-Yvette, France

Philippe Garcia
CEA/DEN/CAD/DEC/SPUA/LMP, CEN Cadarache, F13108 Saint-Paul-Lez Durance, France

(Received 18 October 2014; accepted 26 February 2015)

This work is an overview of the physical approaches required for characterizing and understanding the long-term evolution of ceramics under irradiation. Because this subject is complex and has many ramifications, we have chosen to address the problem by looking at the behavior of a number of key ceramics. In the first part of this work, we present the physical mechanisms responsible for the production of primary defects, pointing out the main differences between metals, semiconductors, and insulators. In part two, we attempt to show how devoted experimental techniques can combine with transmission electron microscopy and x-ray techniques to provide a clearer picture of the long-term evolution of the microstructure of ceramics under irradiation. The last part of this work is devoted to discussing different approaches to explain and describe the long-term behavior of irradiated ceramics.

I. INTRODUCTION

A great deal of research has focused in the past 60 years on understanding and describing the short- and long-term behavior of metals and alloys under irradiation. This in-depth understanding of the behavior of alloys subjected to harsh environments (neutron fluxes, corrosive surroundings, high temperatures, etc.) was spurred on by the development of electricity generating nuclear systems such as Candu, pressurized water reactors, and fast breeder reactors which all include metallic structural materials such as the fuel cladding and pressure vessel. The focus on materials' related issues in relation to electricity generation has gradually turned toward the permanent disposal of nuclear waste, the proliferation of nuclear weapon technologies and materials, and the sustainability of a once-through nuclear fuel cycle. In addition, the effective utilization of nuclear power will require continued improvements in nuclear technology, particularly in relation to safety and efficiency. There are many areas that require the performance of ceramics to be understood and improved. To name but a few of the relevant ceramics and corresponding applications: boron carbide used as neutron absorbing material, silicon and metal carbides as cladding material for future nuclear plants and accident tolerant concepts, oxide fuels for high burn up applications (UO_2), mixed plutonium and minor actinide oxides and carbides for fourth generation nuclear plant (GENIV) fuels, inert matrices for storage of nuclear wastes (pyrochlores, spinels, ZrO_2, MgO), SiC fiber-reinforced SiC composites and other ceramics used as first-wall materials for fusion reactors.[1]

Fundamentally, differences between ceramics and metals are due to differences in the nature of the bonds between atoms. Metals and metallic alloys exhibit no band gap and the ionic charges of the nuclei are screened by electrons: they may be described as a sea of electrons facing a background of positive charges. Thermally activated and radiation induced diffusion results from atomic jumps of

Contributing Editor: William J. Weber
[a)]Address all correspondence to this author.
e-mail: david.simeone@cea.fr
DOI: 10.1557/jmr.2015.77

 © Materials Research Society 2015

https://doi.org/10.1557/jmr.2015.77 Published online by Cambridge University Press

these neutral interstitials and vacancies. Under irradiation, both neutral vacancies and interstitials are created as Frenkel pairs in metals. These Frenkel pairs may agglomerate to produce extended defects. With regard to metals, the development of ab initio and molecular dynamics (MD) calculations nowadays can give a quantitative description of the formation energies of both point and extended defects such as dislocations. On the strength of these atomic scale descriptions, predictive thermodynamic models are now available to describe the phase stability of alloys,[2] including under irradiation.[3]

The complex nature of chemical bonds, partly ionic and partly covalent, even metallic in the case of metal carbides,[4] has for long precluded any similar approach for ceramics. Actually, the term "ceramics" (derived from the Greek word "keramos" meaning pottery) is in itself misleading since it covers a broad range of refractory materials from insulators to metallic solids. These peculiar bonds produce materials which in certain cases exhibit a band gap responsible for the formation of complex charged defects. Iono-covalent ceramics are either insulators exhibiting large band gaps such as zirconia, spinels, and pyrochlores, or semiconductors with small band gaps such as SiC, B_4C, or UO_2. However, this is not an unequivocal criterion for distinguishing metals from ceramics. For instance, metal nitrides and carbides considered as ceramics do not possess a band gap. However, these ceramics exhibit a weak electron density at their Fermi level. The existence of a band gap has far reaching implications. Defects with charged and neutral states may be created at some specific energy level in the band gap. Hence, calculating the band gap of a ceramic accurately (in which standard density functional theory (DFT) often fails[5]) is a prerequisite to any predictive approach to the formation energies of these defects and their concentrations. Whereas in metal, impurities have little incidence on defect energetics, in ceramics they modify the position of the Fermi level and hence have a major impact on these energies.[6]

An additional complication with ceramics stems from the existence of several sublattices that produce the broad diversity of crystalline structures in contrast to essentially cubic and hexagonal structures in metals and alloys. For ionic ceramics, vacancies can be created on both cation and anion sublattices. Pairs or trios of vacancies which satisfy the electroneutrality condition are known as Schottky defects that are often the most stable defects in halides, like NaCl, and oxides, like UO_2.

As for the case for metals and alloys, the excess energy due to dopants or charged defects produced under irradiation can be accommodated by the formation of extended or complex defects in ceramics. Examples of electrically neutral dislocation lines or loops are common.[7–9] Complex defects such as Willis clusters in UO_2[10] are created in situations where the defect concentration increases, e.g., when deviation from stoichiometry increases, to relax the repulsive forces between anions. Because ceramics are usually refractory materials with high melting points, the temperatures at which they equilibrate with their surroundings are much greater than in the case of metals. Hence, reliable measurements on the formation energies of point defects are difficult to perform. If one adds to this the complex defect landscapes that largely depend on the amount of impurities in the pristine ceramic or the difficulties in characterizing point defect nature and concentration in situ, then the task of constructing a comprehensive macroscopic description of the material is bound to have an extremely uncertain outcome. Nonetheless, multiscale approaches are needed to incorporate atomic scale information into accurate models describing relevant phenomena across multiple length and time scales. Such models with a sound physical basis are only just emerging.[11]

Despite the difficulties inherent to the existence of a band gap and the challenge it poses to well-established quantum approaches, it is a paradox that this characteristic actually provides experimental benefits as it enables probing these materials at the atomic scale using powerful spectroscopic techniques such as Raman and luminescence spectroscopy. These techniques offer a unique opportunity to track local symmetries and charged defects but unfortunately cannot be applied to determine the nature and concentration of defects in metal carbides and graphite. Coupling these spectroscopic techniques with synchrotron (x-ray) and neutron sources provides structural information at atomic and nanometric scales simultaneously. These recent experimental advances in association with cutting edge computational tools have a key role to play in understanding the long-term evolution of ceramics subjected to radiation. In turn they could prove to be a tremendous accelerator for progress in fundamental materials and chemical sciences, thus bridging the gap between basic scientific approaches and the development of advanced nuclear energy systems.

A number of reviews[12–15] related to radiation effects in ceramics have been published over the years. The specific aim of the present paper is to emphasize the underlying physics at the atomic and nanometric scales specific to some ceramics subjected to radiation damage. We will provide an overview of some of the more important theoretical and experimental requirements for describing primary radiation damage as well as the long-term behavior of archetypal ceramics used in the nuclear industry, focusing especially on the most recent and promising developments. We focus on a restricted number of materials that exemplify a particular class of phenomena. Crucial issues relating to radiation damage in glasses,[16] clays,[17–19] and graphite[20,21] must unfortunately remain beyond the scope of this paper.

https://doi.org/10.1557/jmr.2015.77 Published online by Cambridge University Press

The first part of this work is devoted to a discussion of primary radiation damage production, pointing out differences and indeed similarities with metallic systems. The second part deals with specific characterization techniques which may be used to track point defects and structural modifications in ceramics. X-ray diffraction techniques are highlighted. Based on a review of microstructural observations, we attempt in the last part of the work to draw a comprehensive picture of the challenges, experimental as well as theoretical, for a control of the long-term microstructural evolution of ceramics.

II. PRIMARY DAMAGE

The main characteristic of radiation damage is the ability of a neutron or charged particle flux to induce multiple collisions in materials at the atomic scale. For crystalline metals and ceramics, neutrons as well as impinging ions and electrons lose their kinetic energy in numerous collisions with target atoms. During these collisions, a large amount of the kinetic energy of the projectile is transferred to atoms initially at rest. Because the energy transfer to these atoms (few tens of kiloelectron volts) is larger than the binding energy in the solid (a few electron volts), atoms will be ejected from their initial positions and proceed to produce in turn more point defects. These collision sequences will last a few tens of picoseconds and drastically increase the amount of defects expected from thermodynamic equilibrium at a given temperature or in a given chemical environment. The nature and concentration of defects produced a few picoseconds following a collision with the high-energy particle (neutron, swift ion, or electron) are termed primary damage and is highly localized in well-defined areas called displacement cascades. The inhomogeneous distribution of primary defects (Frenkel pairs, antisites and Schottky defects or even dislocation loops) over a few nanometers is the main characteristic of radiation damage.

A. Threshold displacement energy (TDE) in ceramics

The most important physical parameter describing this primary damage in a crystal is the TDE. This physical quantity represents the minimum energy that must be transferred to an atom in the crystal for a stable Frenkel pair to be formed. Such a definition was also extended to ceramics. The TDE is independent of temperature and approximately one order of magnitude greater than the cohesive energy of the crystal. It can be understood as the minimum energy required for an atom to be ejected at a distance larger than the recombination radius. However, these energetic considerations do not take into account the kinetic aspect of the process. No one migration path leads to a stable Frenkel pair which results in a certain degree of scatter in the experimental data, in part attributable to the crystal orientation with respect to impinging ions. By analogy with resistivity measurements performed on metals,[22] the dependence of the threshold displacement energies upon crystal orientation[23] was further applied with some degree of success to TDE measurements in carbides like TaC.[24] However, the TDE can be derived from direct in situ observations/electron irradiations of ceramics in conjunction with various spectroscopic techniques such as optical absorption (OA), positron annihilation (PAS), Rutherford backscattering (RBS), and electron paramagnetic resonance (EPR). From single crystal studies, the TDE may be mapped against crystal orientation. However, few ceramics have been experimentally studied and Table I provides available data[14,33] for some relevant oxides and carbides along with some of the calculated values.

From the analysis of these data, there is no obvious dependence of this fundamental quantity neither upon the nature of atomic species of target solids nor crystal structure. As a result, it is doubtful that any correlations may be extracted between TDEs and cohesive energies or crystalline structure. It must be noted that no TDE values have been determined from direct measurements in the case of the following metal carbides and nitrides: ZrN, ZrC, and TiC.[48] Spectroscopic methods are liable to provide us with the most accurate TDE values but they are only sensitive to charged defects in the band gap. High-voltage electron microscopy (HVEM) studies remain the most commonly used tools to estimate TDE in ceramics. They are usually derived from the observation of extended defects and this method may not be entirely straightforward or reliable. For instance, in cerium oxide as will be seen later,[46] the presence of charged oxygen dislocation loops is assumed and oxygen TDEs derived based essentially on indirect, albeit convincing evidence. Also, it is possible that displacement of the oxygen sublattice occurs but does not necessarily lead to the formation of dislocation loops or stacking faults. This may lead to overestimating this crucial quantity. These caveats, along with the dependence of TDEs upon crystal orientation, may be the cause of the rather large scatter observed in the data reported in Table I.

Complementary to these experimental approaches, numerical simulation techniques such as MD have been extensively used. Using empirical pair potentials, it appeared possible to monitor the formation of stable point defects. This technique was applied to the computation of stable defect configurations in ceramics, mainly in oxides.[26,28,34,35,45,49,50] Over recent years, some MD calculations were performed to compute displacement threshold energy in more complex oxides such as pyrochlore[51] ($Y_2Ti_2O_7$) and zircon[50] ($ZrSiO_4$). Table I also reports displacement threshold energies computed using MD.

https://doi.org/10.1557/jmr.2015.77 Published online by Cambridge University Press

TABLE I. Comparison between measured and calculated threshold displacement energies of some ceramics.

	Energy (eV)	Anisotropy	Method
α-Al_2O_3 (corundum)	E_{Al} = 18; E_O = 76	Not known	OA[14,25]
	E_{Al} = 20; E_O = 50	...	...
	E_{Al} = 27.7; E_O = 54.3	$[10\bar{1}0]$	Calculated[26]
UO_2	E_U = 40; E_O = 20	Not known	HVEM[27]
	E_U = 52	[100]	Calculated[28]
	E_U = 85; E_O = 16	[110]	Calculated[28]
	E_U = 46; E_O = 28	[130]	Calculated[28]
TiO_2 (rutile)	E_{Ti} = 50	...	OA[29]
	E_O = 39 ± 4	...	Calculated[30,31]
	E_{Ti} = 80 ± 5; E_O = 85 ± 5	[001]	Calculated[32]
	E_{Ti} = 115 ± 5; E_O = 50 ± 5	[100]	Calculated[32]
	E_{Ti} = 100 ± 5; E_O = 60 ± 5	[110]	Calculated[32]
	E_{Ti} = 160 ± 5; E_O = 70 ± 5	[111]	Calculated[32]
MgO	E_{Mg} = 60; E_O = 64	...	OA[33]
	E_{Mg} = 55; E_O = 55	...	...
	E_{Mg} = 136	[100]	Calculated[34]
	E_{Mg} = 90; E_O = 64	[131]	Calculated[34]
	E_{Mg} = 58.7	[100]	Calculated[26]
	E_{Mg} = 87.7; E_O = 91.7	Average	Calculated[35]
BeO	E_O = 76	Not known	HVEM[36]
6H–SiC (hexagonal)	E_C = 20; E_{Si} = 93	[0001]	PAS, EPR[37]
	E_C = 18–19	$[000\bar{1}]$	OA[38]
	E_{Si} = 30–35	...	RBS[39]
	E_C = 31 ± 1; E_{Si} = 120 ± 1	[0001]	Calculated[40]
	E_C = 65 ± 1; E_{Si} = 35 ± 1	$[000\bar{1}]$	Calculated[40]
	E_C = 54	Not known	HVEM[41]
3C–SiC (cubic)	E_{Si} = 25	[100]	PAS, EPR[37]
	E_{Si} = 25	[100]	OA[42]
	E_C = 31; E_{Si} = 36	[100]	Calculated[40]
	E_C = 38; E_{Si} = 71	[011]	Calculated[40]
	E_C = 28; E_{Si} = 113	[111]	Calculated[40]
B_4C	E_C = 20; E_B = 20	Not known	HVEM[43]
$MgAl_2O_4$	E_O = 60; E_{Al} = 60	Not known	OA[33]
	E_O = 60	...	OA[44]
CeO_2	E_{Ce} = 48; 46; 63	[100]; [110]; [111]	Calculated[45]
	E_O = 20; 33	[100]; [110]	Calculated[45]
	E_{Ce} = 44–58	Not known	HVEM[46]
	E_O < 33	Not known	HVEM[46]
c-ZrO_2 (YSZ)	E_{Zr} = 54.5; 54; 68.5	[100]; [110]; [111]	Calculated[45]
	E_O = 14; 30; >100	[100]; [110]	Calculated[45]
	E_{zr} = 80	Not known	EPR[47]
	E_O > 120	Not known	EPR[47]

However, it must be borne in mind that the charge on cations can vary substantially with position even in simple oxides. In α-Al_2O_3 with a simple hexagonal structure, it was shown experimentally that the charge associated with Al cations varies from 2.35 in its standard position to 0.65 in an interstitial position.[52]

The parameterization of the interatomic pair potentials then appears as a key point in these simulations. In the formal charge approximation, the charge associated with cations and anions is fixed and fitted to describe Coulomb interactions adequately. For MgO, the TDEs for Mg were found to be equal to 136 and 90 eV along the [100] and [131] directions respectively, and reaches 64 eV along the [131] direction for O ions.[34] Comparison of these values with experimental results reported in Table I is not particularly good. The ratio between the cation and anion displacement threshold energies simulated is twice the experimental values for MgO.[34] In alumina, the values of 28 and 54 eV are reported for aluminum and oxygen ions along $[10\bar{1}0]$ (in hexagonal notation), respectively[26] in disagreement with the corresponding experimental data in Table I. Since pair potentials appear to lack reliability in predicting experimental values, authors have resorted to fitting potentials to reproduce them adequately.[49] Such an approach does not ensure that fitted potentials with fixed charges for anions and cations can reproduce other properties such as the hierarchy of stable defects. MD simulations using empirical potentials may differ significantly from ab-initio methods in the determination of TDE, as found for SiC.[53]

It is important to note that no electron exchange is allowed with empirical interatomic potentials in classical MD calculations. The use of charge variable potentials depending on the local environment[54,55] seems to be an alternative way for a more realistic computation of TDEs in ceramics, or rather a complementary method to resource consuming ab initio calculations. However, ab initio MD simulations were recently performed[45] to take into account the role of charge transfer during the displacement process.

B. Topology of displacement cascades and defect production

Despite the limitations inherent to MD simulations, the time-dependent distribution of energy and defects produced in a displacement cascade was extensively used to describe the topology of cascades in ceramics.[56,57] For high-energy primary knock on atoms (PKAs) with a kinetic energy of a few hundreds of kiloelectron volts, the displacement cascades separate into dense subcascades within a few picoseconds following the primary collision as occurs in metals.[58] This is not surprising because the energy of displaced atoms is so large that displacement is hardly affected by the nature of chemical bonds in the solid. When the PKA energy decreases below a few tens of kiloelectron volts, a single cascade is created[59] in agreement with other investigations.[60] An example of such an approach was applied at the beginning of the century to discuss the structural stability of spinels and pyrochlores under irradiation. Calculations of defects in spinel structures were performed to investigate the effect of mass and the initial amount of disorder in pristine samples (antisite defects on cation sublattices) on the topology and the amount of primary damage production.[61] These authors performed MD simulations on three different spinels $MgAl_2O_4$ (M_{Al} = 27) exhibiting no antisite defects on the cation

https://doi.org/10.1557/jmr.2015.77 Published online by Cambridge University Press

sublattices, $MgGa_2O_4$ (M_{Ga} = 70) in which Mg and Ga atoms are present in both sublattices and $MgIn_2O_4$ (M_{In} = 114) where half of the In cations lies on the Mg sublattice. The authors also computed average concentrations of antisite defects at the end of simulations. The results are summarized in Fig. 1.

Even if the density of defects in the core of the cascades seems to be more important for In than Mg spinels, no drastic difference is observed on cascade morphology. The amount of oxygen vacancies and interstitials as well as the number of cation antisite defects does not seem to evolve with the degree of antisite defects in pristine spinels. These results are illustrated in Fig. 2. In this example, it appears that the amount of disorder in pristine spinels has little impact on the production of point defects. There is experimental evidence that in yttrium-stabilized zirconia (YSZ), which displays a cubic structure, the amount of native oxygen vacancies (controlled by the yttria content) has no significant effect on the production of F^+-type centers involving oxygen atom displacements through elastic collisions, in spite of large recombination volumes.[47] However, very few studies are available to extend this analysis to other ceramics.

MD simulations based on interatomic pair potentials performed on complex oxides such as spinels, zircon, and pyrochlore clearly show that Frenkel, antisite, and Schottky defects can be created under irradiation in each sublattice. Also, the number of Frenkel pairs and antisite defects follows a power law of the PKA energy with an exponent less than 1. For covalent materials, more sophisticated interatomic potentials as the Tersoff potential[62] describing oriented bonds were used to simulate

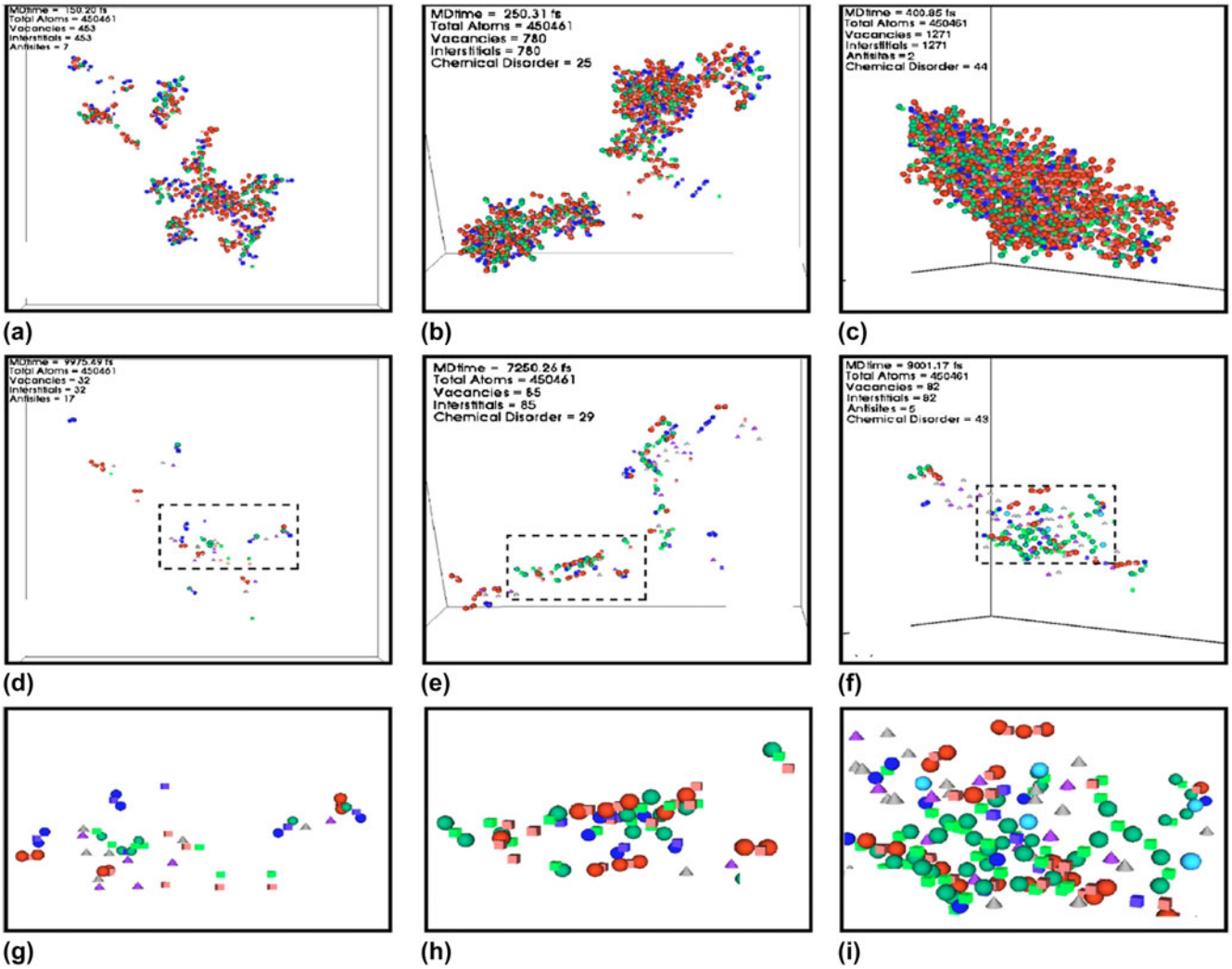


FIG. 1. Snapshot of displacement cascades generated by a 5 keV PKA in the three spinels showing the displacement of ions at the end of the collisional phase of the cascade. (a) 150 fs and (d, g) 9975 fs, for a normal $MgAl_2O_4$ spinel and Al PKA; (b) 250 fs and (e, h) 7250 fs, for a half-inverse $MgGa_2O_4$ spinel and Ga PKA; (c) 400 fs and (f, i) 9001 fs, fully inverse spinel, $MgIn_2O_4$ and In PKA (c, f, and i are zoom-ins of the core of the cascades). Blue spheres are associated with Mg interstitials, green spheres are associated with B (Al, Ga, In) interstitials, cubes denote cationic vacancies, and red spheres denote oxygen atoms in perfect sites. Nominal charges for cations and anions were used in the simulation.[61]

https://doi.org/10.1557/jmr.2015.77 Published online by Cambridge University Press

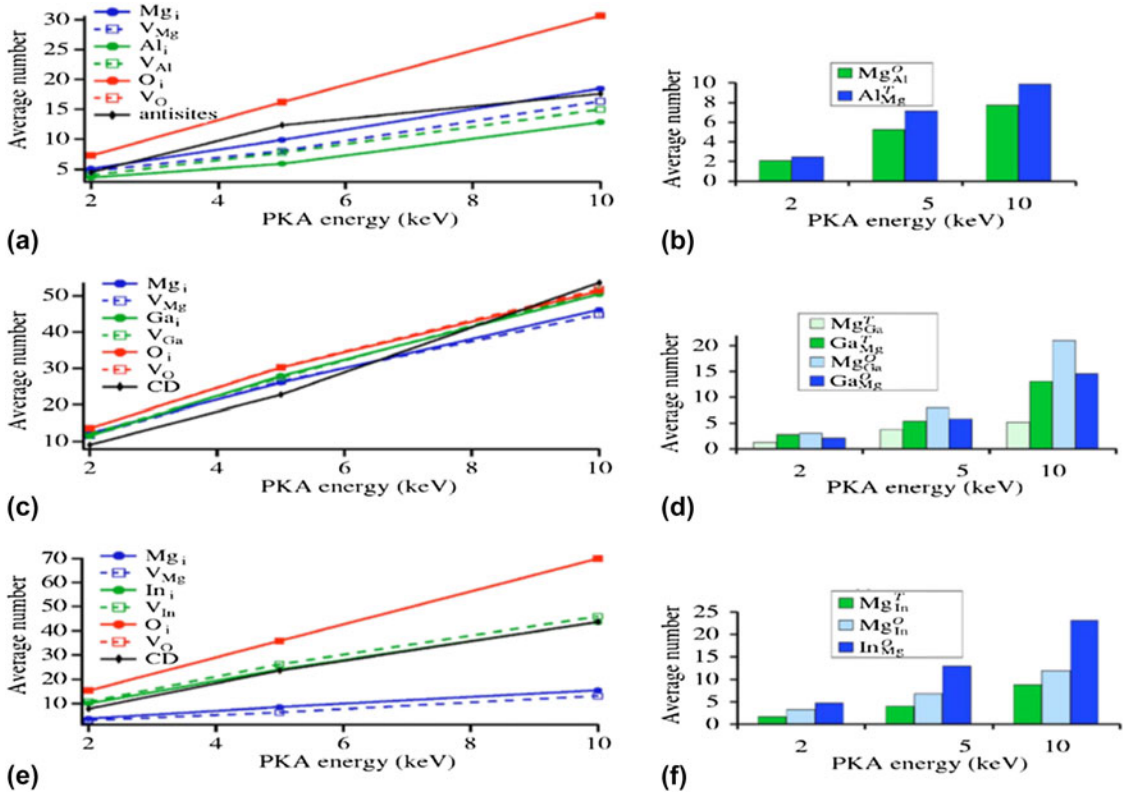


FIG. 2. Average number of interstitials, vacancies, and antisite/cation disorder defects created at energies of 2, 5, and 10 keV in a (a) normal $MgAl_2O_4$, (c) half-inverse $MgGa_2O_4$, and (e) inverse $MgIn_2O_4$ spinel. The average number and type of cation disorder defects and their coordination are shown in (b), (d), and (f) figures. The superscripts *T* and *O* refer to tetrahedral and octahedral coordination, respectively.[61]

displacement cascades. This type of interatomic potential was successfully used to describe cubic and hexagonal SiC.[63,64] Again simulations indicate[64] that the number of surviving defects (Frenkel pairs, Schottky pairs, antisites, and small clusters) follows a power law of the PKA energy. These results are similar to those encountered in metals. The exponent of the power laws depends on the nature of the ceramic studied and the type of defect.

To understand the effect of crystal structure or the nature of bonds on the production of primary defects, it is common and helpful to calculate the ratio of the surviving Frenkel pairs at the end of a displacement cascade, derived from calculations or experiments, over the calculated (BCA) number of defects. A question naturally arises: in ionic crystals, Does this efficiency depend upon the choice of interatomic potentials? Recent ab initio MD simulations of SiC[65] reveal that charge transfer is significant during the displacement of knocked-on Si and C atoms. This charge transfer modifies the energy barrier for the formation and migration of stable defects. However, these calculations remain so far too time consuming to be extended to high-energy PKAs and to compare the amount of Si and C clusters produced to classical MD simulations.

Zinkle first estimated this efficiency in oxides from OA experiments. However, this analysis was based on oxygen vacancies (F centers) measured at low temperature[14] ($T_{irr} < 80$ K) in Al_2O_3 and MgO.[66] He supposed in his analysis that the number of oxygen vacancies is the signature of Frenkel pairs on the anion lattice. Moreover, he assumed that there was no migration of point defects in the displacement cascade at the irradiation temperature. Zinkle showed that there is no clear dependence of this efficiency with the PKA energy in Al_2O_3. Figure 3 displays the evolution of this efficiency extracted from experiments and calculations for Al_2O_3 and SiC.

As regards the Al_2O_3 results however, it is possible that oxygen vacancies are also due to the formation of Schottky defects. Some more recent RBS results[67] relating to Al_2O_3 seem to contradict the previous analysis of Zinkle and show a distinct effect of PKA energy upon the defect production efficiency. One possible reason for this disagreement may be related to the fact that the number of defects derived from RBS measurements probably cannot be ascribed to single oxygen interstitials only. It is no doubt related to the presence of complex defects such as dislocation loops.[68] This illustrates the difficulty involved in determining from experiments accurate data for primary defects in ceramics.

The relative independence of this efficiency with the PKA energy in Al_2O_3 may be understood as the signature

https://doi.org/10.1557/jmr.2015.77 Published online by Cambridge University Press

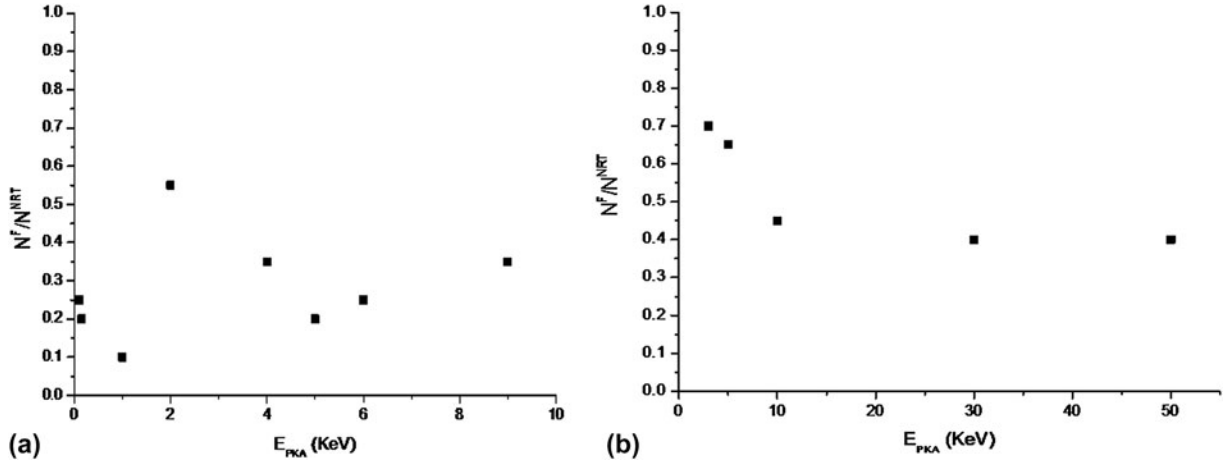


FIG. 3. Variation in the ratio of the number of surviving Frenkel pairs over the number of Frenkel pairs estimated by the NRT formula in (a) Al_2O_3,[14] and (b) SiC[65] versus the energy of PKA.

of Coulomb interactions between charged stable defects produced in the displacement cascades. It must be noticed that MD simulations performed on MgO with fixed charges for anions and cations[69] do not reproduce experimental results.[66] The disagreement between simulations and experiments suggests that charge transfer between atoms in MgO during multiple collision events in displacement cascades has a substantial effect. If charge transfer occurs while atoms are at saddle positions, then the apparent energy barrier required to form stable defects may decrease thereby modifying the amount of stable defects. This charge transfer effect has already been observed and discussed in Si[55] and more recently in SiC.[65]

These results show that both the topology of a displacement cascade as well as the evolution of associated primary defects need to be more clearly understood in ceramics. Variable charge MD simulations or/and ab initio MD simulations[70] may provide useful tools for understanding the impact of crystal structure on the topology of displacement cascades and may help explain discrepancies between experimental results and MD simulations performed using empirical interatomic potentials.

C. Impact of inelastic collisions on primary damage

The production of stable defects due to elastic collisions can be described since the corresponding mechanisms at the atomic scale are relatively well defined and well known. On the other hand, the production of defects by inelastic collisions in materials, i.e., the slowing down of high-energy PKAs by multiple collisions with electrons in matter, results from indirect and complex mechanisms is not fully understood.[71] The concept of displacement cascades can no longer be used to describe the changes of materials irradiated with such swift heavy ions, i.e., with a kinetic energy above a few megaelectron volts per unit of atomic mass such as fission products in UO_2. For insulator materials with wide band gaps, inelastic collisions produced by these swift heavy ions, whether followed by self-trapped exciton formation as in SiO_2[72,73] or not, induce defect production in halides, silicates, and carbonates as reported from numerous experimental studies.[74] The analysis of these experimental results enabled Clinard and Hobbs to outline a few favorable conditions for the creation of defects via inelastic interactions[74]:

(i) The electronic excitations, like polarons or excitons, must be localized over a few atomic sites.
(ii) The available energy in the excitation must be comparable to the displacement threshold energy.
(iii) The lifetime of the excitation must be of the order of the lattice vibration (>0.1 ps) to allow coupling with the motion of atoms.
(iv) Non-radiative transitions must prevail over radiative transition, i.e., luminescence.

Obviously, metals do not satisfy conditions (i), (ii), or (iii) and so are in the main insensitive to electronic excitations. In small gap semiconductors, the energy given to electrons during inelastic collisions is much smaller than the TDE. Even if collective excitations created by the electric field of the impinging ion involve a greater energy, these excitations are not localized. This implies that the first condition is not fulfilled. These materials seem to be insensitive to inelastic excitations. However, athermal melting of silicon by laser beams may be accounted for by the lattice instability following a critical amount of the above band-gap electronic excitations[75] as expected from the Coulomb explosion mechanism.

In insulators, the energy of electronic excitation is about 10 eV. As a result, inelastic collisions can create defects in ionic compounds with small TDEs. Two distinct

https://doi.org/10.1557/jmr.2015.77 Published online by Cambridge University Press

processes may lead to the creation of defects: the self-trapped exciton formation like in halides and silica[76] and the creation of a deep hole associated with Auger de-excitation.[77] In alkali halides,[71,78,79] self-trapped excitons associated with the electronic excitation dissociate into a hole and an electron leading to the formation of stable color centers.[80] Excitons are also responsible for the creation of oxygen Frenkel pairs in pure SiO_2.[81,82] Ab initio calculations reveal a coherent scenario for this mechanism.[83] Such a mechanism is possibly responsible for the phase separation and the oxygen bubble formation observed in silicate glasses.[16]

On the other hand, deep holes[77] produced in the cation sublattice formed by metals of columns IV and V of the Mendeleev table vanish leading to the formation of positive or neutral oxygen atoms that are able either to desorb or create oxygen clusters. Such a mechanism explains the reduction of many oxides observed when subjected to electronic excitation irradiations. Anionic desorption from alkali halides and alkaline-earth oxide surfaces arises from bi-exciton production by electronic excitations with laser beams.[84]

Defect creation is not the only effect induced by an inelastic energy transfer in ceramics. It is well known[71,73] that inelastic effects largely modify the mobility of defects enhancing it under certain circumstances. The seminal work by Bourgoin and Lannoo clearly showed that this inelastic energy transfer largely affects the diffusion of point defect in semiconductors.[55,85,86] Similar effects such as a-thermal point-defect recombination have also been reported for SiC from calculations and experiments.[87] In oxides, a large amount of experimental data is available. It appears that inelastic energy transfers induce an annealing of radiation damage in oxides like Al_2O_3 and MgO.[88] Until now, a clear description of the physical mechanisms responsible for the large modification of the microstructure, like the formation of colloids in MgO irradiated with electrons[89] or the conflicting role of the electronic excitation in the nucleation or growth of loops in Al_2O_3/MgO system[90] is unavailable. It must be noted that the impact of inelastic energy transfers on the diffusion of defects strongly seems to depend on the amount of impurities in the insulator.[73]

Moreover, one must bear in mind that for swift heavy ions with a high inelastic stopping power (>10 keV/nm), the intense electric field produced by the impinging ion creates a high density coherent excitation of electrons that are able to produce some damage even in pure metal,[91] via some poorly elucidated mechanism. No attempts are made up to now to point out the impact of such an intense electric field on phase transition in insulators.

Despite many attempts since the beginning of the 50s at describing the impact of electronic excitation, i.e., the slowing down of swift ions through some energy transfer to electrons, there is still no universally accepted model at the microscopic scale.[73] Different models have been proposed to capture some aspects of the underlying physics behind this process. The most physical model is the Coulomb spike model.[92] In this approach, swift heavy ions create a highly ionized cylindrical region ejecting valence and core electrons during ion-electron collisions by well-known processes.[93] Repulsive electrostatic forces between ions induce a strong deformation of the lattice before electroneutrality is restored on the femtosecond time scale. Despite some attempts,[91] a quantitative model based on this mechanism is difficult to establish because of the difficulty in calculating a realistic electric field in the ionized cylinder.[94]

A step further was achieved with the thermal spike model.[95,96] In this two-step approach, the energy lost by the swift ions in the ionized cylinder by inelastic collision is first transferred to electrons via a simple heat equation on the femtosecond time scale. In this approach, more complex phenomena for energy transfer to electrons such as multiple ionizations or Auger emission are neglected. The electron gas in the ionized cylinder is described by an "electronic" temperature T_e. In a second stage, it is assumed that the electron–phonon coupling induces a transfer of the heat to the lattice on a picosecond time scale. This two temperature model, derived from laser–matter interaction studies, was introduced to explain plastic deformation, the so-called "hammering effect", of amorphous ceramics like SiO_2[97]; point defect and defect cluster formation in ionic crystals like LiF[98] and CaF_2[99]; or amorphization in SiO_2 quartz[97] irradiated with swift heavy ions. Despite the fact that the two temperature model appears to describe adequately the morphology of tracks observed in some ceramics,[100] the use of two diffusion equations to determine the temperatures in the electron gas and in the lattice is not clearly justified. In addition, coupling between the electronic and the ionic temperatures which results from electron–phonon coupling is assumed somewhat arbitrarily linear.[96] During the last decade, this two temperature model was combined with MD simulations to handle radiation damage induced by swift heavy ions in ceramics.[101] The interest in and limitations of this simulation approach is still the subject of discussion but its success stems from the relative ease with which one may discuss in a quantitative way synergetic effects between elastic and inelastic energy deposition and their impact upon the production of primary defects in insulators and semiconductors.

III. SPECIFIC CHARACTERIZATION TECHNIQUES ASSOCIATED WITH THE STUDY OF IRRADIATED CERAMICS

In insulators and semiconductors, the existence of a band gap results in the formation of various stable atomic defects with different charge and spin states. This enables

https://doi.org/10.1557/jmr.2015.77 Published online by Cambridge University Press

detecting these defects using particular spectroscopic techniques such as EPR and/or OA with exceptional sensitivities. In this case, modifications of high-energy bands (above 1000 cm^{-1}) provide accurate information about chemical rearrangements. These techniques are extensively used to study radiation-induced chemical changes in clays and SiC and can also be used to track structural modifications. Low-energy bands (below 1000 cm^{-1}) collected in infrared and Raman ranges give accurate information about the local modification of symmetries induced by atomic relaxations. Complementary neutron and x-ray diffraction techniques were extensively used to study structural modifications (phase transformation, variation of chemical composition, or amorphization, etc.) or gather microstructural data (strain field, polygonization of grains, etc.). Of course, transmission electron microscopy (TEM) offers, as for studies involving metals and alloys, a unique opportunity to obtain snapshots of the irradiated microstructure. In addition to structural information which can be obtained from electron diffraction, it also has the precious advantage of constituting a direct "observation" of the microstructure.

A. EPR and OA spectroscopic techniques

In insulators and semiconductors, charged defects are produced in the band gap. This effect is at the origin of the term color center that designates neutral or charged vacancies or interstitials in ionic crystals. In particular, paramagnetic F centers (neutral anion vacancies with one trapped electron) were thoroughly investigated in alkali halides and to a lesser degree F and F^+ centers in oxides like MgO and Al_2O_3[102] with EPR and OA. More recently, an extensive study was carried out on F^+-type centers in YSZ produced by elastic collisions induced by electron and ion irradiations as for MgO.[103] Hole centers produced by electronic excitations with charged particle or photon irradiations can also be detected by these techniques with great sensitivity, like the V^- centers produced in MgO.[102] Figure 4 displays an example of EPR spectra collected on irradiated YSZ single crystals.

EPR spectra allow detecting a small amount of electronic spins $\sim 10^{16}$ irrespective of sample volume. Moreover, the different charge states of paramagnetic species can be sorted out on the basis of the specific *g*-tensor principal values and hyperfine splitting. Angular dependence of the *g*-factor and hyperfine coupling constant can also provide valuable information about point-defect anisotropy. However, interference with EPR signals of paramagnetic impurities is always possible. For wide band gap materials, combining the EPR signal with OA and photoluminescence spectra may lift uncertainties. A great deal of work has been devoted to tracking point defects induced by irradiation in ceramics using OA as in $MgAl_2O_4$.[44,104] Although defects can be more directly studied in iono-covalent materials than in metals, the presence of both cation and anion sublattices

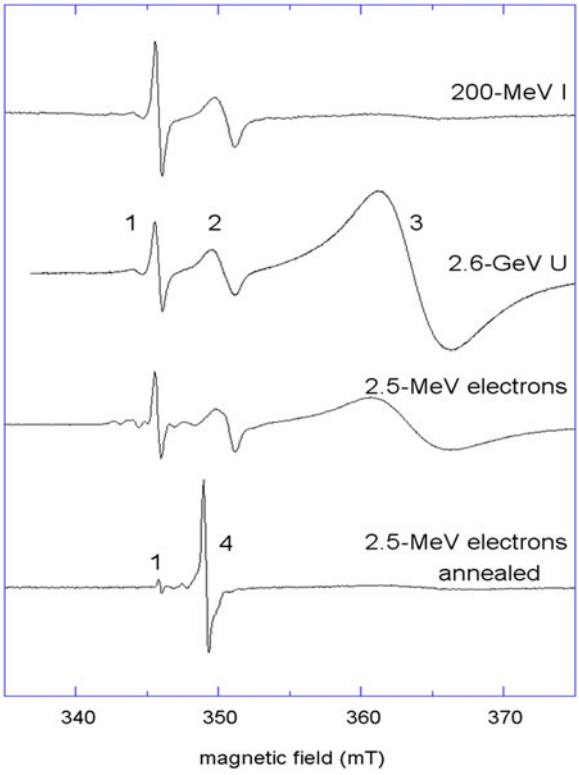


FIG. 4. RT-EPR spectra for B//<100> of YSZ (100) single crystals irradiated under 200-MeV I ions at 1×10^{13} cm^{-2}, 2.6-GeV U ions at 1×10^{13} cm^{-2}, and 2.5-MeV electrons at 2.9×10^{18} cm^{-2}, annealed at 973 K: lines 1–2 and 1–4 were assigned to F^+-type centers, whereas line 3 was associated with T-centers (Zr^{3+} ions in trigonal point symmetry).[47]

and the multiplicity of possible charge states make the number of basic defects much more important.

These spectroscopic techniques are extensively used to characterize defects produced by irradiation in silicates but do not give any indication about the local distortion they are liable to induce and accompanying structural modifications. To illustrate this point, Fig. 5 shows a correlation between the volume fraction of the tetragonal phase produced by irradiation in monoclinic zirconia[105] and the amount of F^+ centers measured by OA in the material.[106]

Because these spectroscopic techniques are bulk sensitive techniques, they do not provide any spatial resolution. Raman and infrared spectroscopic techniques, sensitive to phonon vibrations, can give some clues on relaxations associated with the creation of defects. The study of peaks above 1000 cm^{-1} has shown the existence of Si–Si and C–C bonds in irradiated SiC.[107,108] Low-energy peaks (below 1000 cm^{-1}) also give accurate information in relation to structural modifications of crystal structures induced by low-energy ions or in the wake of swift heavy ions.[109] This technique was applied to demonstrate that pure monoclinic zirconia is transformed into tetragonal zirconia under ion-beam irradiation[110] and track defects in UO_2 irradiated with low-energy particles.[111]

https://doi.org/10.1557/jmr.2015.77 Published online by Cambridge University Press

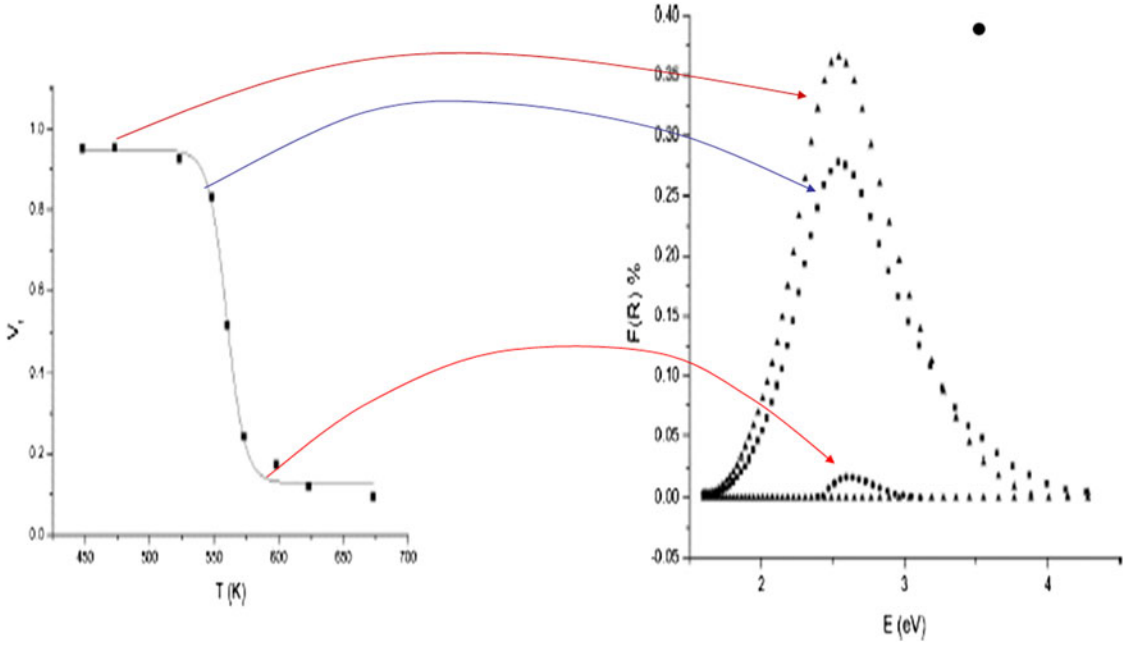


FIG. 5. Correlation between the tetragonal volume fractions of m-ZrO_2 sample irradiated at room temperature under a flux of 10^{10} cm^{-2} s^{-1} by 800 keV Xe ions determined from XRD measurements (left graph) and the amount of oxygen vacancies (F^+ centers). Comparison between these two graphs clearly points out that the tetragonal volume fraction is associated with the existence of these charged defects in irradiated pure monoclinic zirconia. Copyright 2004, The American Physical Society. Reproduced with permission from Ref. 105.

B. Diffraction techniques

Different diffraction techniques are used to track modifications in the long-range order of ceramics subjected to radiation damage. TEM is commonly used in studies devoted to the analysis of the microstructure of ceramics under irradiation. This technique can provide a clear insight into mechanisms involving radiation damage and snapshots of the microstructure in real space. Figure 6 shows the impact of the implantation profile on the c-SiC microstructure obtained from a cross-sectional TEM micrograph of SiC irradiated with Au ion beams of different energies.

The contrast arising from local changes in diffracting conditions enables measuring strain fields. However, the main feature of this technique is a direct determination of the space group from the collected diffraction patterns. Combining diffraction and direct observation of the microstructure, it is possible to point out specific domains. This bright field analysis was applied to study the zirconia transformation induced by irradiation.[105] Nowadays, high-resolution transmission electron microscopy (HRTEM) offers the unique opportunity to extract information over a typical size of a few nanometers. The detailed structure of radiation-damaged areas is generally blurred though due to the high local strains induced by the presence of defects. In conventional TEM, this makes it difficult and impossible to find appropriate diffraction conditions to select equivalent atomic rows with precision. HRTEM images, showing rows of atoms, enable the study of stacking faults and dislocation loops in ceramics by selecting very small areas[46] and the method was applied to discuss phase transformations in spinel.[112,113] Because the energy momentum transfer vector $\boldsymbol{q} = \boldsymbol{k}_{\mathrm{scatt}} - \boldsymbol{k}_{\mathrm{inc}}$[114] ($\boldsymbol{k}_{\mathrm{scatt}}$ and $\boldsymbol{k}_{\mathrm{inc}}$ are the wave vectors associated with the scattering and incident wave, respectively), is large in electron diffraction experiments (few hundreds of nm^{-1} for 400 kV microscope) compared with x-ray radiations (few tens of nm^{-1} for Cu K_α radiations), energy filtering TEM in combination with an imaging technique offers the opportunity to collect diffraction patterns over a large q range. For polycrystalline samples with substantial mosaicity, it is then possible to apply the kinematic theory of diffraction neglecting multiple scattering and then compute a pair distribution function (PDF). PDFs are of prime importance for the study of amorphization in irradiated ceramics and the method has been used to discuss amorphization in SiC.[115] HRTEM also offers the opportunity to apply quantitative spectroscopic techniques like electron energy loss spectroscopy,[116] high angular resolution electron channeling,[117] or electron dispersive x-ray spectroscopy to quantify the concentration of species in ceramics over few nanometers.[118]

The main limitation of TEM is due to the fact that observations must be performed on thin films. Because the foils used in TEM are only a few hundreds of nanometers thick, the observed microstructure is not necessarily representative of the bulk. Free surfaces are powerful sinks,[119]

https://doi.org/10.1557/jmr.2015.77 Published online by Cambridge University Press

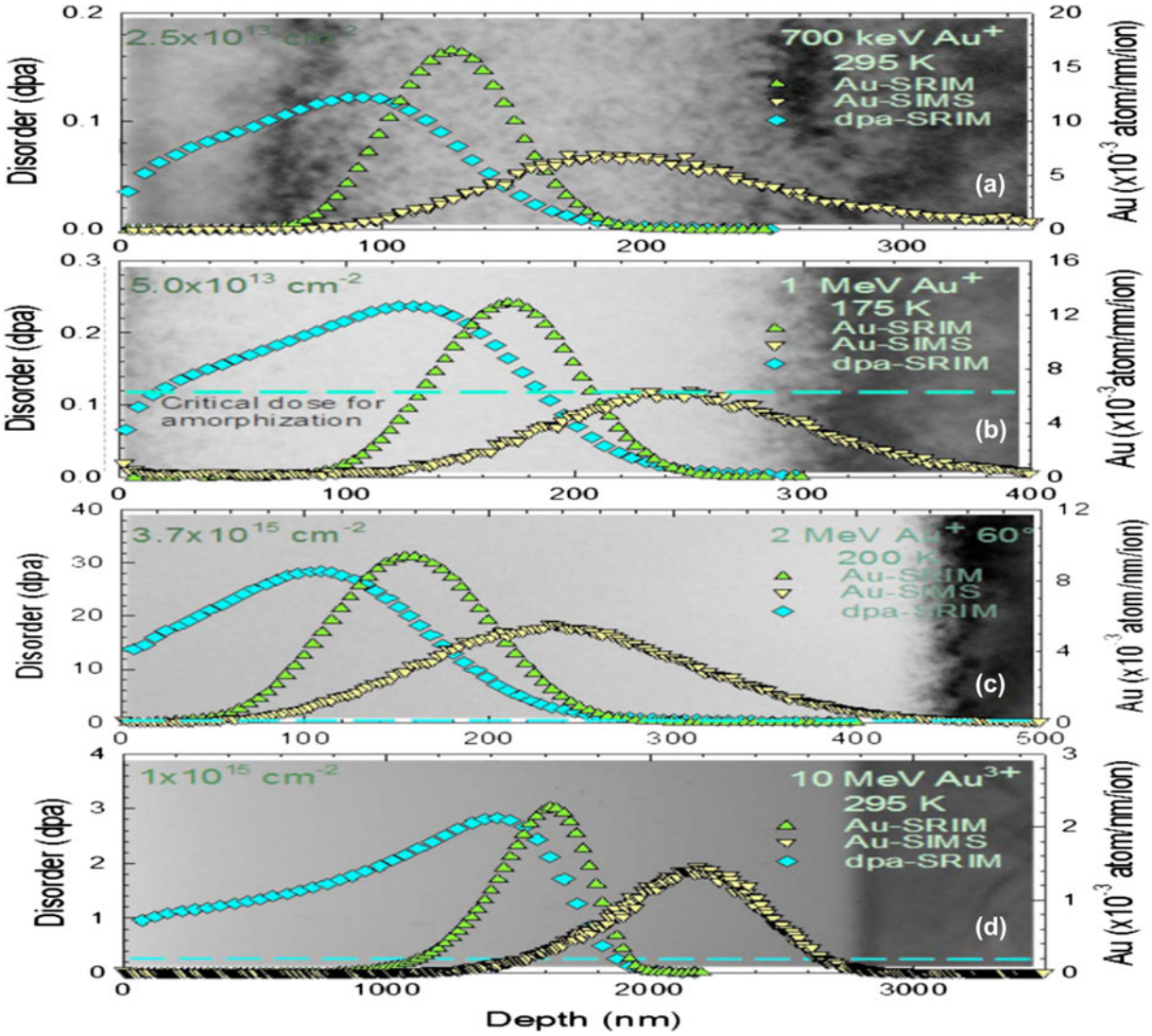


FIG. 6. SRIM predictions and SIMS measurement are superimposed upon TEM images for (a) 700 keV Au^+ irradiation in 6H–SiC at 295 K under a flux of 10^{10} cm^{-2} s^{-1} to an ion fluence of 2.5×10^{13} cm^{-2}, (b) 1.0 MeV Au^+ irradiation at 175 K to an ion fluence of 5×10^{13} cm^{-2}, (c) 2.0 MeV Au^+ irradiation with 60° incidence angle at 295 K to an ion fluence of 3.7×10^{15} cm^{-2}, and (d) 10 MeV Au^{3+} irradiation at 295 K to an ion fluence of 10^{15} cm^{-2}. Diamond-shaped boxes indicate the SRIM calculated damage profile. The triangle-shaped boxes indicate the Au profile in units of atoms per nanometer and per ion. The dashed line indicates the critical dose value for amorphization.[108] Discrepancies between SRIM simulations and SIMS measurements are discussed in detail in the original paper. Copyright 2005, AIP Publishing LLC. Reproduced with permission from Ref. 108.

which are able to substantially modify point defect concentrations as they annihilate there. The effect of this artifact on the microstructure is difficult to assess and obviously depends on the material studied. As ceramics studied in the nuclear industry possess high melting points, diffusion of point defects in the thin foils is limited at cryogenic or room temperature. It must also be noticed that the electron beam impinging the surface of the sample is also liable to enhance the surface diffusion of light elements (Li, Mg, Al). Because TEM is a diffraction technique,[114] it possesses a resolution window which is small (below 1 nm) and large clusters cannot be observed. Moreover, unit cell parameters obtained from TEM diffraction patterns are not accurate. Unit cell determination, atomic positions, and composition changes in irradiated ceramics can be obtained from the analysis of x-ray and neutron diffraction patterns collected on polycrystalline samples for which the kinematic approximation of diffraction applies. For polycrystalline samples, microstructural changes like strain fields and/or characteristic size of coherent diffracting domains can also be obtained. Moreover, diffuse scattering has long been applied to track point defect induced strain fields in irradiated single crystals. However, the analysis of diffuse scattering maps induced by defects is not straightforward. Figure 7 displays the elastic strain induced by the formation of lithium nanocrystals in Li_2O

https://doi.org/10.1557/jmr.2015.77 Published online by Cambridge University Press

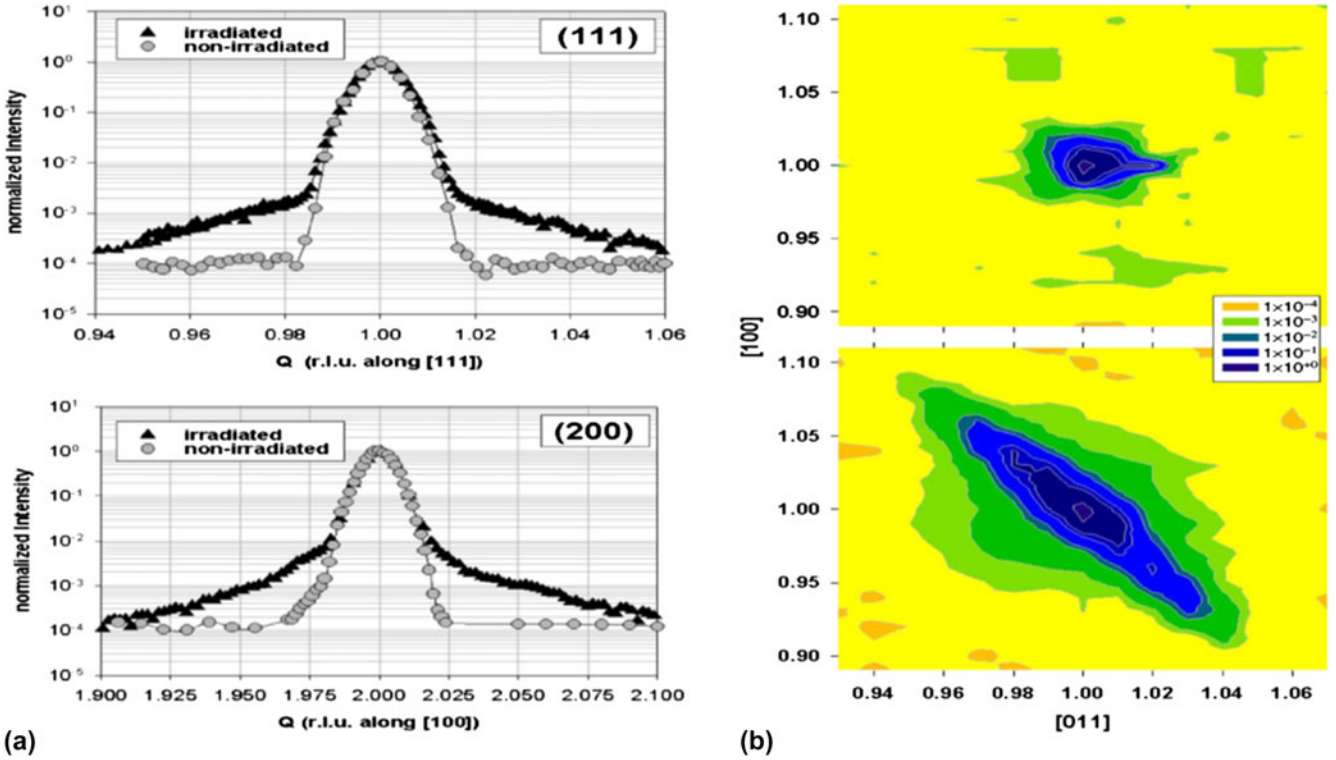


FIG. 7. (a) Comparison of the scattering intensity (on a logarithmic scale) observed in irradiated Li_2O at room temperature by 1 MeV electron beam under a flux of 10^{11} cm^{-2} s^{-1} and nonirradiated Li_2O along radial scans through the (111) and (200) peaks. In the reference sample, the peak shape is a Gaussian upon a flat background whereas scattering due to distortion is visible following the electron irradiation 123. (b) Normalized iso-intensity contours of elastic diffuse scattering around the (111) peak of a nonirradiated (top) and an irradiated (bottom) crystal of Li_2O. The large ellipsoid in blue is the signature of a large strain field induced by Li nanoclusters. Copyright 2003, The American Physical Society. Reproduced with permission from Ref. 120.

single crystals irradiated with electrons. Because of the large penetration depth of x-rays and neutrons, such analyses must be performed on single crystals or polycrystalline samples irradiated over a large volume (few micrometers).[120] Thus, this technique does not allow determining the effect of damage induced by defects in solids irradiated with low-energy ions because the damaged volume remains always smaller than the x-ray penetration depth (or the extinction length for single crystals).

To track the structural and microstructural evolution of ceramics irradiated with low-energy ions, the glancing incidence x-ray diffraction (GIXRD) technique may be used.[121] By adjusting the incidence angle of the x-ray beam, it is possible to characterize radiation damage over a length scale of a few hundreds of nanometers, which is the typical depth over which damage is induced with low-energy ions. Specific features and limitations of this technique have been discussed.[122] The analysis of Bragg peaks collected in GIXRD provides information on the structure and the microstructure (strain field, coherent diffracting domains, etc.). Figure 8 displays the variation of diffraction patterns collected as a function of depth on irradiated m-ZrO_2 samples. The analysis of these diffraction patterns is a means of quantifying the radiation-induced monoclinic-to-tetragonal phase transformation in pure zirconia.[121]

Spinel transformations[121] and the evolution of metallic carbides[48] have also been studied this way. In this approach, the Rietveld method is used to refine diffraction patterns. Moreover, it also offers the opportunity to probe the impact of radiation damage over large space scales (few nanometers) due to its large coherent volume.[122] However, this method then fails to track radiation-induced amorphization. The development of new synchrotrons may offer the opportunity to determine accurate PDFs from total scattering measurements.

From this rapid discussion, it appears that many powerful experimental tools are now emerging to probe the nature and amount of defects induced by irradiation as well as structural and microstructural changes associated with the presence of excess defects.

IV. LONG-TERM MICROSTRUCTURAL EVOLUTION OF CERAMICS

As in metallic materials, irradiation induces drastic modifications of the microstructure, point defect

https://doi.org/10.1557/jmr.2015.77 Published online by Cambridge University Press

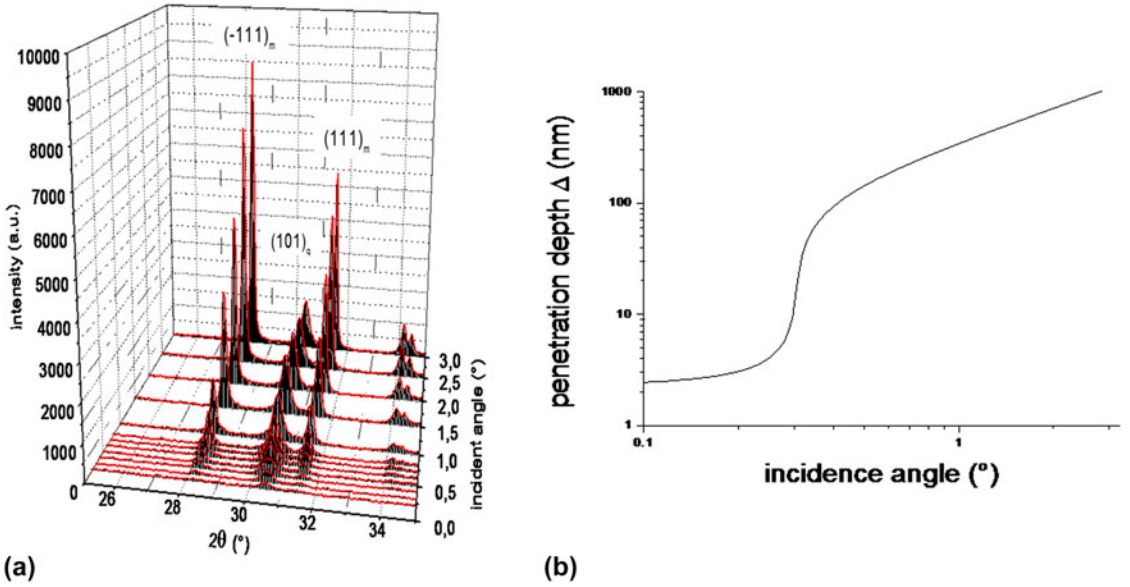


FIG. 8. Variation of the diffraction patterns (a) of m-ZrO_2 irradiated with 800 keV Ar ions at room temperature under a flux of 10^{10} cm^{-2} s^{-1} and a fluence of 10^{14} cm^{-2} s^{-1} collected at different incidence angles associated with different penetration depth of the x-ray beam (b). From the analysis of these diffraction patterns, the volume fraction of the tetragonal phase produced under irradiation can be extracted and compared with the damage profile extracted from simulations.[121]

production and clustering, phase transformations and amorphization. However, due to the complexity of chemical bonds and crystalline structures, the predictions of long-term radiation-induced microstructural changes are scarce in ceramics compared with metals and alloys. The number of systems and initial microstructures, the range of irradiation conditions (characteristics of incident charged particles, temperature, and atmosphere) make this topic difficult to review comprehensively although this has been attempted in the past.[123] Our aim here rather than a comprehensive review is to show, through various examples taken from a range of different materials (MgO, α-Al_2O_3, UO_2, CeO_2, ZrO_2), some of the aspects that make these metal oxide systems very different from alloys.

A. Irradiation induced microstructural evolutions in "simple" oxides and radiation induced diffusion

The combination of high-energy electron irradiations and subsequent or simultaneous observation in a high-voltage transmission electron microscopy[25,124] provides a unique insight into basic radiation effects since electrons are liable to produce point defects only. Using electrons for inducing damage greatly simplifies the system in comparison with situations where cascades are produced, as can be the case with ions or neutrons. This type of experiment bears the added attraction of enabling a selective displacement of atoms lying on one or the other sublattice, in cases where displacement energies of the metallic element are substantially different from that of oxygen.[8,27] In their study of α-Al_2O_3, Stathopoulos and Pells[8] irradiated thin foils at temperatures ranging between 300 and 1100 K with 300 keV electrons, which is above the electron energy required to displace aluminum ions (175 keV) but significantly below that required to displace oxygen ions (390 keV). They observed the formation and growth (above 800 K) of interstitial dislocation loops of stoichiometric composition lying on basal or prismatic planes. Because only cation defects are produced upon irradiation, the formation of a stoichiometric dislocation loop requires the movement of oxygen ions to occur in which electrostatic interactions must play a key role. The authors propose a scenario to explain their observations involving first an aggregation of Al ions between either basal or prismatic planes subsequent to which oxygen ions diffuse into the defect structure to form the stable loops. This first example illustrates the close relationship between primary defect production and charged defect diffusion properties. It is reasonable to assume here that electrostatic interactions may induce cooperative effects between the oxygen and metal sublattices.

More recently, basic studies have been carried out on the CeO_2 fluorite structure considered to be a surrogate for UO_2.[9,46] The afore-mentioned authors irradiated thin CeO_2 foils with electrons in the 200 keV to 3 MeV energy range and at temperatures between 300 and 1073 K. In the lower energy range (200–500 keV), presumably lower than that required to displace Ce atoms from their sites, they observed the formation of larger dislocation loops characterized by a very strong strain contrast. The loops

https://doi.org/10.1557/jmr.2015.77 Published online by Cambridge University Press

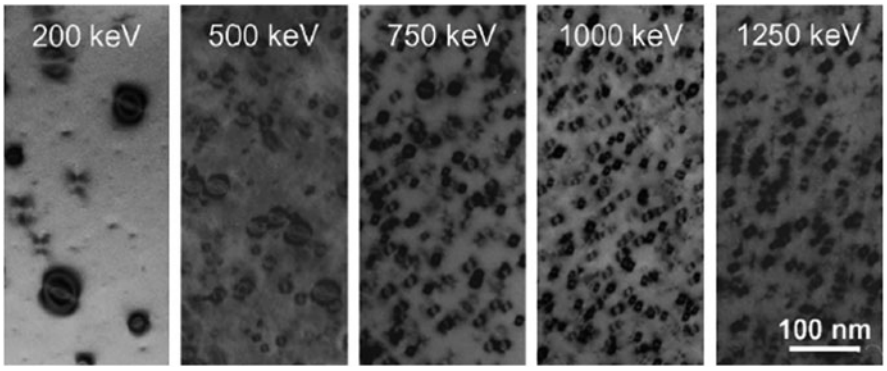


FIG. 9. BF-TEM images of nonstoichiometric interstitial type loops in CeO_2 irradiated with different energy electron beams, indicating for the left-hand micrograph in particular, unusually marked strain contrast. Copyright 2008, Elsevier. Reproduced with permission from Ref. 46.

shown in Fig. 9 are lying on {1 1 1} planes with a Burgers vector parallel to the <1 1 1> direction. These extended defects are assumed by the authors to result from the insertion of a layer of oxygen atoms based on two arguments: the electron energy lies well below that required to displace cerium ions and HRTEM observations indicate a stacking fault but the absence of an additional layer of cerium atoms. One may also add that the large strain fields observed in the lattice are an indication that the dislocation loops are charged.

This latter point has been extensively reported with regard to YSZ also in the work of Yasuda et al.[125] They irradiated YSZ samples with low-energy ions such as 300 keV O^+ ions and subsequently re-irradiated them with low-energy (200 keV) electrons, i.e., again below the threshold energy for displacing zirconium ions. In doing so, they observed the very rapid growth of large defect clusters (roughly 1 nm/s), which induced a considerable strain field as would be expected from a charged defect cluster. The defect reaches a threshold size (roughly 1 μm) and then breaks down into a dislocation tangle. The process of nucleation, growth, and breakdown of defects repeats itself under continued electron irradiation. These results are interpreted by the authors as resulting from the formation of charged oxygen platelets possibly involving electronic excitation effects inferred from the unexpectedly high mobility of oxygen point defects.

Ryazanov et al.[126] have attempted to interpret observations by Yasuda et al.[125] based on rate equations which take charge effects into account explicitly. In this work, the authors show how an internal electric field may be created in the vicinity of the charged oxygen dislocation, electric field which in turn gives rise to an additional stress field around the dislocation. The authors consider a diffusion equation for free electrons, coupled with the electrical potential created around the charged defect cluster. The theoretical loop growth rate is compared to experiment. Charge accumulation is assumed to take place on the loops which trap free electrons that are created as a result of the interaction of the sample with the impinging electron beam. As a result of the concomitant accumulation of oxygen atoms and electrons, the induced strain around the defect rises until the yield stress is reached and plastic deformation occurs through dislocation multiplication.

We have seen how a selective displacement of a given lattice may be a means of producing charged extended defects that require taking into account Coulomb interactions over a longer range than when point or extended defects are neutral. However, it is interesting to note that in many cases, when the energy of impinging electrons increases or when ion beams or fission fragment recoils are used either producing displacements on both sublattices or full damage cascades, interstitial dislocation loops appear to be stoichiometric in character. This is reported to be the case in α-Al_2O_3,[127] MgO,[128] CeO_2[46] for electron energies above 1250 keV, UO_2[7,27] for fission fragment induced damage and for high-energy electrons above 1.6 MeV.[129]

In the case of MgO, Kinoshita et al.[130] have attempted to model the microstructural evolutions in electron-irradiated foils based on chemical rate theory equations. These were adapted from models developed for metals by taking into account point defect formation and diffusion specific to both sublattices. The authors derive from confrontation of theory with TEM observations migration energies of interstitials and vacancies. Stoichiometric loops are assumed.

In MgO[128] and in fluorite UO_2[7,27,131] and CeO_2,[46] perfect interstitial dislocation loops are reported which have a (1/2) <1 1 0> Burgers vector and lie in neutral {1 1 0} planes. One of the major differences observed between the work of Yasunaga et al. on CeO_2 and the work of Soullard on UO_2 is that in the latter case there is no sign of oxygen loops even below the electron energy required to displace uranium atoms (1.6 MeV). However, it is worth mentioning that the studies were carried out 30 years apart. The fact that the interstitial loops formed

https://doi.org/10.1557/jmr.2015.77 Published online by Cambridge University Press

are stoichiometric, as is reported in these studies, requires that charged interstitials be trapped in stoichiometric proportions. This is difficult to conceive since in the fluorite structure materials UO_2 and CeO_2, cations have much lower diffusion coefficients than anions, and much greater migration energies. This was recently confirmed from DFT calculations.[132] So, if growth is controlled by the slower of the two species, then charge accumulation must occur on the loops. In addition, in Soullard's work,[27] the high-energy electron irradiation experiments were carried out at room temperature and interstitial loops are observed to multiply and grow as the electron fluence increases demonstrating that uranium interstitials migrate. In fact, Soullard proposes an estimate for the migration energy of the uranium interstitial of roughly 0.3 eV, albeit based on a large number of hypotheses. The lowest interstitial migration energy found for uranium by Dorado et al.[132] was 4.1 eV and involved an indirect mechanism. Such widely differing migration energy values may suggest either a charge transfer effect or cooperative effects between the oxygen and uranium sublattices. In the former case, the charge transfer would drastically reduce the migration barrier of the defect, as suggested for the migration of neutral oxygen interstitials in ZrO_2.[52] Cooperative effects between the oxygen and uranium sublattices have been shown to decrease the uranium vacancy migration barriers in UO_2.[132]

A word must be said about radiation induced or enhanced diffusion. In metals, simplified rate theory approaches have adequately explained results from experiments seeking to characterize this phenomenon.[133] Under simplifying assumptions of homogeneously distributed point defect sinks, rate equations for both vacancies and interstitial atoms are set up and solved assuming that a steady state situation is reached. The defect production rate is balanced off by the rates at which defects recombine (mutual recombination) or are eliminated at sinks of prescribed concentration (elimination of point defects at fixed sinks).

Two limiting cases were derived. At lower temperatures, under steady state conditions controlled by mutual recombination of Frenkel pairs, the enhanced diffusion coefficient is proportional to the square root of the defect production rate. The activation energy is given by half the migration enthalpy of the slowest moving point defect. At high defect sink concentrations however, where concentrations are controlled by the rate at which defects are eliminated at internal sinks, there exists a range of temperatures in which enhanced diffusion is independent of temperature and proportional to the defect production rate. To what extent does this theory also apply to cations or anions in oxide systems?

Van Sambeek et al.[131] carried out mainly oxygen radiation enhanced self-diffusion experiments in MgO in a wide range of temperature and fluxes and analyzed

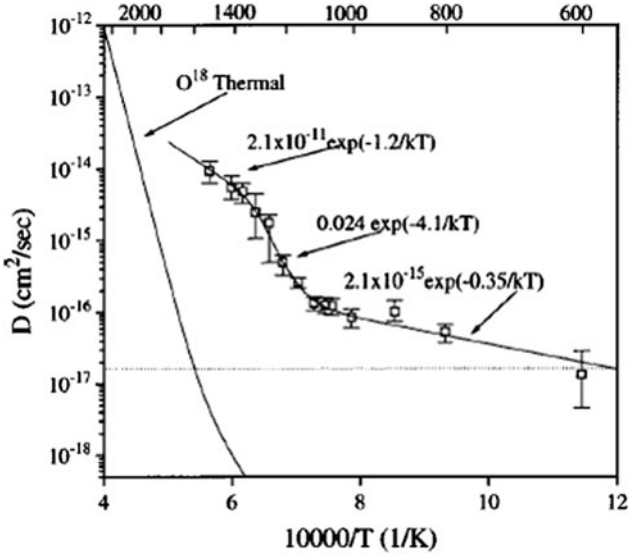


FIG. 10. Arrhenius representation of radiation-enhanced oxygen self-diffusion coefficients subjected to a 2 MeV Kr ion irradiation in MgO. Dashed lines represent ballistic mixing and continuous lines represent thermally activated diffusion. Copyright 1998, AIP Publishing LLC. Reproduced with permission from Ref. 131.

their results in the light of this theory. Figure 10 illustrates some of the most relevant results. Only in the higher temperature range is it possible to relate convincingly the temperature and ion flux dependence of the diffusion coefficient to one of the two limiting cases above: square root dependence of diffusion coefficient upon ion flux with an activation energy approximately half that of the vacancy migration energy. In this case, recombination-limited diffusion is apparent. In an intermediate-temperature range, the higher than expected activation energy was interpreted by the authors as the dissociation energy of small vacancy clusters. At lower temperatures, the diffusion coefficients nearly exhibit a linear dependence upon flux and low activation energy are compatible with sink limited recombination. Why the two rate limiting cases should occur in reverse order with respect to metals is unclear but it appears from this work that the adaptation of rate models for metals to oxides requires further effort. The different range of interactions between mobile defects and fixed, possibly charged dislocations must constitute a major difference with metals that models based on rate theory should take into account.

To conclude this section, we have seen that one of the major differences between oxides and metals lies in the existence of both charged point and extended defects. The formal charge of point defects may vary depending upon temperature and irradiation conditions and migration barriers can be very sensitive to that. Frenkel pair recombination volumes are also generally much greater than in metals due to the long-range Coulomb interactions. Under certain conditions also, dislocation loops appear to be

https://doi.org/10.1557/jmr.2015.77 Published online by Cambridge University Press

charged, inducing uncommonly high strain fields around them and creating an additional length scale determined by electrostatic interactions. Any predictive approach to these microstructural effects seems to require additional equations describing the conservation of defects on both sublattices along with the conservation of electrons and holes taking into account the dielectric material properties. Such approaches, which should be supported by first principles and MD, are far from common and only limited contributions may be found in the literature.

From an experimental point of view, more basic data on different oxide systems are definitely required to help sort through the incredibly complex picture and pick out general trends and important factors. A good starting point has to be radiation-induced diffusion studies in which microstructural evolutions and atom movement are intimately connected and have the power to provide a comprehensive picture of the material behavior.

B. Phase transformation and amorphization induced by irradiation

Under irradiation, ceramics are constantly subjected to damage accumulation and annealing as a result of the creation of defects and their elimination as they diffuse to sinks or annihilate. Their response to these opposing forces (damage accumulation and restoration) is varied: some ceramics retain their crystal structure or even recrystallize (UO_2), others undergo phase transformations (such as pure zirconia) or amorphize (such as certain pyrochlores). We are firstly concerned here with providing the reader not only with a feel for the incredible wide variety of responses of ceramics to irradiation but also with ascertaining whether a rationale may be drawn from this complex picture. The follow-up to this is the identification of areas that require more attention if we are to arrive at a reasonably predictive approach to these important long-term radiation-induced consequences.

A great deal of work has focused on oxides which have representatives in all the four classes of response (damage accumulation with conservation of structure, recrystallization, phase transformation, and amorphization).

Symmetry and compacity are attributes which are extremely favorable to radiation resistance. As seen in the previous section, rocksalt (MgO), fluorite (YSZ, CeO_2, UO_2, PuO_2) or hexagonal oxides (α-Al_2O_3), i.e., oxides in which anions and cations occupy all Wyckoff positions, appear to have no alternative under irradiation but to establish smaller scale patterns of themselves: they form stoichiometric, interstitial dislocation loops that grow into dislocation networks. These materials are possibly good candidates for testing traditional rate theory approaches but the essentially unexplained fact remains that radiation enables atomic movement that would otherwise be completely insignificant (see Sec. IV. A).

Another type of response to radiation observed is the structural transformation from a lower to a higher symmetry phase and an interesting example is pure zirconia which has three different phases: monoclinic, tetragonal, and cubic (YSZ). This oxide goes through a displacive phase transition as the temperature rises from a monoclinic to a more symmetric tetragonal phase. Similarly, under irradiation and irrespective of the nature of the energy deposition, pure zirconia shows the same transition which has been ascribed to a strain field induced by the accumulation of F^+ centers. These defects are formed in all the three types of zirconia, but if irradiation of the tetragonal phase proceeds further, the material does not change to the cubic phase.[105] In fact, there are reports that nanograined pure tetragonal zirconia is subject to amorphization probably because of large local strain fields[134] produced by the increasing F^+ centers. The reason for this is no doubt that unlike the monoclinic phase, the tetragonal phase is not sensitive to the strain field.

Radiation tolerant $MgAl_2O_4$ responds yet differently. Under certain high-energy irradiation conditions, dislocation loops are indeed observed,[117] but they are not under irradiation conditions (mainly low-energy ions) similar to those alluded to the above for zirconia, single phase MgO, or α-Al_20_3 (of which $MgAl_2O_4$ spinel may be considered a binary compound). This is thought to be due to the fact that antisite defects[110] (Mg on Al sites and vice versa) can form in spinel and experimental evidence for this has been well supported by MD simulations.[61] Similar results[110] were observed on $MgCr_2O_4$ and $ZnAl_2O_4$ which may themselves be considered as $MgO–Cr_2O_3$ and $ZnO–Al_2O_3$ binary oxide compounds. The spinel example is an illustration that the crystal structure, and more specifically, the number and nature of sublattices that make up the ceramic can play an important role in controlling its long-term microstructure. Note that antisite defect or dislocation loop formation does not exempt these oxides from amorphization. $MgAl_2O_4$ single crystals irradiated with 400 keV Xe ions lose their long-range order at low temperature (100 K) and high doses (25 dpa). A similar loss of long-range order is observed in α-Al_2O_3 irradiated with 1.5 MeV Xe ions at 20 K and 4 dpa, illustrating that strain fields resulting from irradiation can be responsible for amorphization, irrespective of what actually induces the strain field in the first place (antisites, dislocation loops, or F^+ centers in the case of tetragonal ZrO_2). Increasing the irradiation temperature is expected to decrease the steady state defect concentration under irradiation, with obvious consequences on the threshold dose required for amorphization.

Pyrochlores, composition $A_2B_2O_7$ where A and B are cations, have a distinct tendency to amorphize when they are not able to disorder to a more symmetric and stable fluorite phase, such as occurs with $Gd_2Zr_2O_7$ or $Am_2Zr_2O_7$.[135,136] The irradiation conditions that lead to amorphization are very much dependent upon the nature

https://doi.org/10.1557/jmr.2015.77 Published online by Cambridge University Press

of A and B cations and an interpretation was given based on the accumulation antisite defects.[56] Antisite defects indeed produce very large local strains which the Li and Johnson formalism,[137] used to interpret the crystal to glass transition, predicts may lead to amorphization. Based on a wide range of TEM observations[137] of ion-irradiated pyrochlores of different compositions and supported by MD calculations, the authors claimed that the key parameter was the ratio of the two cation atomic radii; quantity which determines the level of strain induced by antisite defects,[56,138] hence the propensity of a pyrochlore to amorphize. In this approach, the authors[56,138] do not account for the relaxation of the crystal structure when calculating antisite defect energies.

Several alternative interpretations of the amorphization process have emerged more recently. One is based on MD[42] calculations which appear to indicate that it is driven by the formation of B–B dumbbells in displacement cascades; covalent bonding being conducive to amorphization. The explanation for the amorphization of pyrochlores is similar to the structural freedom approach developed by Gupta[139] and applied by Hobbs[140] to the stability of glasses under irradiation. The other involves the oxygen sublattice. In the previous interpretations, amorphization of spinels or pyrochlores appears to result from the complete destabilization of the more disordered cation sublattice. However, theories are now emerging in which the authors claim that amorphization of titanium dioxide and pyrochlores[141] is the result of two antagonistic processes: the first involves the removal of oxygen atoms from their original lattice sites by elastic or inelastic collisions and the second the reconstruction of the anion sublattice through diffusion processes. According to these authors, the amount of cation antisites is not the key parameter. Recent ab initio MD calculations[142] seem to confirm this assumption and provide an atomistic picture for pyrochlore amorphization. During the structural transition, O_2-like molecules are formed, and this anion disorder further drives cation disorder eventually leading to an amorphous state.

These studies highlight the complex interplay between both sublattices and its impact on the radiation tolerance of oxides.

For materials exhibiting a large time scale for recombination of point defects resulting from radiation damage, the amount of local distortion will obviously depend upon whether displacement cascades overlap. The multiple impact models firstly derived by Gibbons,[143] were applied by Weber[144] with some degree of success to explain observed amorphization in zircon and SiC. Moreover, some authors also discussed synergetic effect of inelastic and elastic stopping power on the amorphization of SiC[145,146] to discuss fine variations of the amorphization threshold as a function of the incident ion energy.

V. CONCLUSION

The complex nature of bonds between atoms in ceramics leads to a broad range of crystal structures characterized by multiple sublattices. In this report, we provide an overview of the exceptional variety of radiation effects that this induces. The main difference with defects encountered in metals is that they are charged so in addition to basic Frenkel disorder, vacancies, interstitials, and dumbbells, one is also faced with Schottky disorder and a whole gamut of variably charged structures. Because predicting the number of stable defects left over from a damage cascade is an important elementary step toward modeling a microstructure, we first review and discuss experimental data related to this and the propensity of numerical methods to reproduce the data. It transpires that the discrepancies between TDEs measured and those determined from numerical methods probably stem from the fact that MD models usually involve fixed charges and are very sensitive to interatomic potentials. Ab initio MD models provide an encouraging option for capturing some of the charge transfer phenomena and eventually predicting defect concentrations left over from damage cascades. From a computational stand point, the existence of a band gap makes calculating defect energies an extremely complex task from first principles, but experimentally, it enables spectroscopic techniques such as EPR, Raman, or OA to be implemented. The second part of this document is devoted to spectroscopic techniques in particular. Abundant examples of their usefulness in tracking charged defects are given. However, tracking individual defects is insufficient for providing larger scale information of microstructural changes. This is why they should be associated with TEM or specific structural analyses based on x-ray or neutron diffraction. In recent years, with the expansion of synchrotron radiation in particular, a very wide range of techniques has become available and we discuss some of the issues experimentalist are confronted with when attempting to choose the most appropriate option to characterize usually small damaged volumes. The last part is devoted to giving the reader a feel for the incredible range of microstructural evolutions encountered in ceramics. Different types of response to irradiation (loops, antisites, colored centers, etc.) are outlined with various examples of charged structures that require Coulomb interactions to be incorporated in rate theory descriptions. Although no comprehensive theory is yet available for describing the range of higher scale microstructural changes observed in these materials, it is possible to attempt to rationalize matters. Radiation defects induce strain fields that can either lead to a phase transformation to a higher symmetry structure if it is available and sensitive to strain fields, to recrystallization or to full blown amorphization. In oxides, it also appears that several schools of thought exist on what the

https://doi.org/10.1557/jmr.2015.77 Published online by Cambridge University Press

underlying characteristic is, if any, that determines this behavior. In the last ten years, focus has been put on the open cation sublattice that is susceptible to disorder and its contribution to strain-induced amorphization. More recently, approaches have emerged that highlight the importance of damage annealing on the oxygen sublattice. Whatever the explanation, one cannot help thinking that diffusion processes and cooperative effects between the cation and anion sublattices play a key role at several time and length scales. How else could one interpret the formation of neutral dislocation loops in fluorite structures at temperatures that should preclude cation movement?

Until now, the clustering and recombination of defects has only really been tackled qualitatively. This is both because of the difficulties in identifying the basic mechanisms experimentally and because we are still missing microstructural models, based on atomic scale modeling capable of describing damage cascades predictively, that account for the key role of Coulomb interactions.

REFERENCES

1. G.R. Hopkins and R. Price: Fusion reactor design with ceramics. *Nucl. Eng. Des./Fusion* **2**, 111 (1984).
2. F. Ducastelle: *Order and Phase Stability in Alloys* (Amsterdam, Netherlands, 1991).
3. G. Martin and P. Bellon: Driven alloys. *Solid State Phys.* **53–54**, 1 (1997).
4. A. Gusev, A. Rampel, and A. Magerl: *Disorder and Order in Strongly Non Stoechiometric Compounds* (Springer Verlag, Berlin, Germany, 2001).
5. C. Freysoldt, B. Grabowski, T. Hickel, and J. Neugebauer: First-principles calculations for point defects in solids. *Rev. Mod. Phys.* **86**, 253 (2014).
6. J.C. Bourgoin and M. Lannoo: *Point Defects in Semiconductors* (Springer Verlag, Berlin, 1983).
7. A. Whapham and B. Sheldon: Radiation damage in uranium dioxide. *Philos. Mag.* **12**, 1179 (1965).
8. A. Stathopoulos and G. Pells: Damage in the cation sublattice of α-Al_2O_3 irradiated in an HVEM. *Philos. Mag. A* **47**, 381 (1983).
9. K. Yasunaga, K. Yasuda, S. Matsumura, and T. Sonoda: Nucleation and growth of defect clusters in CeO2 irradiated with electrons. *Nucl. Instrum. Methods Phys. Res., Sect. B* **250**, 114 (2006).
10. B.T.M. Willis: The defect structure of hyper-stoichiometric uranium dioxide. *Acta Crystallogr., Sect. A: Cryst. Phys., Diffr., Theor. Gen. Crystallogr.* **34**, 88 (1978).
11. P. Brydon, J. Schmiedt, and C. Timm: Microscopically derived Ginzburg-Landau theory for magnetic order in the iron pnictides. *Phys. Rev. B* **84**, 214510 (2011).
12. L. Hobbs, F. Clinar, S. Zinkle, and R. Ewing: Radiation effects in ceramics. *J. Nucl. Mater.* **216**, 291 (1994).
13. S. Zinkle and E. Hoddgon: Radiation-induced changes in the physical properties of ceramic materials. *J. Nucl. Mater.* **191**, 58 (1992).
14. S. Zinkle and C. Kinoshita: Defect production in ceramics. *J. Nucl. Mater.* **251**, 200 (1997).
15. P. Trocellier, D. Gosset, and D. Simeone: ^{3}He thermal diffusion coefficient measurement in crystalline ceramics by μnra depth profiling. *Nucl. Instrum. Methods Phys. Res., Sect. B* **210**, 507 (2002).
16. S. Peuget, JM. Delaye, and C. Jegou: Specific outcomes of the research on the radiation stability of the French nuclear glass towards alpha decay accumulation. *J. Nucl. Mater.* **444**, 76 (2014).
17. S. Sorieul, T. Allard, G. Morin, B. Boizot, and G. Calas: Native and artificial radiation-induced defects in montmorillonite. An EPR study. *Phys. Chem. Miner.* **1**, 32 (2005).
18. F. Bergaya and G. Lagaly: *Developments in Clay science, Handbook of Clay Science*, Vol. **5** (Elsevier, Oxford, UK, 2013).
19. T. Allard and G. Calas: Radiation effects on clay mineral properties. *Appl. Clay Sci.* **43**, 143 (2009).
20. J. Bonal and L. Gosmain: See for a Review on the Evlution of Stransport and Structural Properties of Graphite Irradiated in Nuclear Plants, Internal Report; CEA, 2004.
21. D. Billington and J. Crawford: *Radiation Damage in Solids*, Vol. **5**, 2nd ed. (Princeton University Press, NY, 1961); p. 396.
22. W. King, K. Merkle, and M. Meshii: Determination of the threshold-energy surface for copper using in-situ electrical-resistivity measurements in the high-voltage electron microscope. *Phys. Rev. B* **23**, 6319 (1981).
23. P. Vajda: Anisotropy of electron radiation damage in metal crystals. *Rev. Mod. Phys.* **49**, 481 (1977).
24. D. Gosset, J. Morillo, C. Allison, and C.H. De Novion: Electron irradiation damage in stoichiometric and substoichiometric tantalum carbides TaC_x part 1: Thershold displacement energies. *Radiat. Eff. Defects Solids* **118**, 207 (1991).
25. G.P. Pells and T. Shikama: Radiation damage in pure and helium-doped α-Al2O3 in the HVEM quantitative aspects of void and aluminium precipitate formation. *Philos. Mag. A* **48**, 779 (1983).
26. R. Williford, R. Davanathan, and W. Weber: Computer simulation of displacement energies for several ceramic materials. *Nucl. Instrum. Methods Phys. Res., Sect. B* **141**, 94 (1998).
27. J. Soullard: High voltage electron microscope observations of UO_2. *J. Nucl. Mater.* **135**, 190 (1985).
28. C. Meis and A. Chartier: Calculation of the threshold displacement energies in UO_2 using ionic potentials. *J. Nucl. Mater.* **341**, 25 (2005).
29. E.C. Buck: Effects of electron irradiation of rutile. *Radiat. Eff. Defects Solids* **133**, 141 (1995).
30. K.L. Smith, M. Collela, R. Cooper, and E.R. Vance: Measured displacement energies of oxygen ions in titanates and zirconates. *J. Nucl. Mater.* **321**, 19 (2003).
31. M. Robinson, N.A. Marks, K.R. Whittle, and G.R. Lumpkin: Systematic calculation of threshold displacement energies: Case study in rutile. *Phys. Rev. B* **85**, 104105 (2012).
32. B.S. Thomas, N.A. Marks, L.R.L. Corrales, and R. Devanathan: Threshold displacement energies in rutile TiO2: A molecular dynamics simulation study. *Nucl. Instrum. Methods Phys. Res., Sect. B* **239**, 191 (2005).
33. G. Pells: Radiation effects and damage mechanisms in ceramic insulators and window materials. *J. Nucl. Mater.* **155**, 67 (1988).
34. B. Park, W. Weber, and L. Corrales: Molecular dynamics study of the threshold displacement energy in MgO. *Nucl. Instrum. Methods Phys. Res., Sect. B* **166**, 357 (2000).
35. L. Kittiratanawasin, R. Smith, P. Uberuaga, and K. Sickafus: Displacement threshold and Frenkel pair formation energy in ionic systems. *Nucl. Instrum. Methods Phys. Res., Sect. B* **268**, 2901 (2010).
36. J. Pigg, A. Garrison, and S. Austermann: Radiation damage in beryllium oxide single crystals. *J. Nucl. Mater.* **49**, 67 (1973).
37. X. Kerbiriou: Silicon displacement threshold energy determined by electron paramagnetic resonance and positron annihilation

https://doi.org/10.1557/jmr.2015.77 Published online by Cambridge University Press

spectroscopy in cubic and hexagonal polytypes of silicon carbide. *J. Nucl. Mater.* **362**, 202 (2007).
38. J.W. Steeds: Transmission electron microscope radiation damage of 4H and 6H SiC. *Diamond Relat. Mater.* **11**, 1923 (2002).
39. W. Jiang: Response of nanocrystalline 3C silicon carbide to heavy-ion irradiation. *Phys. Rev. B* **80**, 161301 (2009).
40. R. Devanathan and W. Weber: Displacement energy surface in 3C and 6H SiC. *J. Nucl. Mater.* **278**, 258 (2000).
41. I.A. Honsvet, R.E. Smallman, and P.M. Marquis: A determination of the atomic displacement energy in cubic silicon carbide. *Philos. Mag. A* **41**, 201 (1980).
42. J. Lefèvre, J.M. Costantini, S. Esnouf, and G. Petite: Silicon threshold displacement energy determined by photoluminescence in electron-irradiated cubic silicon carbide. *J. Appl. Phys.* **105**, 023520 (2009).
43. T. Stoto, L. Zuppiroli, and J. Pelissier: Absence of defect clusters in electron irradiated boron carbide. *Radiat. Eff.* **90**, 161 (1985).
44. G.P. Summers, G.S. White, K.H. Lee, and J.H. Crawford, Jr: Radiation damage in $MgAl_2O_4$. *Phys. Rev. B* **21**, 2578 (1980).
45. H.Y. Xiao, Y. Zhang, and W.J. Weber: Ab initio molecular dynamics simulations of low-energy recoil events in ThO2, CeO2, and ZrO2. *Phys. Rev. B* **86**, 054109 (2012).
46. K. Yasunaga, K. Yasuda, S. Matsumura, and T. Sonoda: Electron energy-dependent formation of dislocation loops in CeO_2. *Nucl. Instrum. Methods Phys. Res., Sect. B* **266**, 2877 (2008).
47. J. Costantini, F. Beuneu, S. Morrison Smith, R. Devanathan, and W. Weber: Paramagnetic defects in electron-irradiated yttria-stabilized zirconia: Effect of yttria content. *J. Appl. Phys.* **110**, 123506 (2011).
48. D. Gosset, M. Dollé, G. Baldinozzi, D. Simeone, and L. Thomé: Structural evolution of zirconium carbide under ion irradiation. *J. Nucl. Mater.* **373**, 123 (2008).
49. J. Crocombette and D. Galheb: Modeling the structure of zircon (ZrSiO4): Empirical potentials, ab initio electronic structure. *J. Nucl. Mater.* **257**, 282 (1998).
50. P. Moreira, R. Devanathan, J. Yu, and W. Weber: Molecular-dynamics simulation of threshold displacement energies in zircon. *Nucl. Instrum. Methods Phys. Res., Sect. B* **267**, 3431 (2009).
51. H.Y. Xiao, F. Gao, and W.J. Weber: Threshold displacement energies and defect formation energies in $Y_2Ti_2O_7$. *J. Phys.: Condens. Matter* **22**, 415801 (2010).
52. E. Kotomin and A. Popov: Radiation-induced point defects in simple oxides. *Nucl. Instrum. Methods Phys. Res., Sect. B* **141**(4), 1 (1998).
53. G. Lucas and L. Pizzagalli: Comparison of threshold displacement energies in β-SiC determined by classical potentials and ab initio calculations. *Nucl. Instrum. Methods Phys. Res., Sect. B* **229**, 359 (2005).
54. A. Rappe and W. Goddard: Charge equilibration for molecular dynamics simulations. *J. Phys. Chem.* **95**, 3358 (1991).
55. F. Streitz and J. Mintmire: Electrostatic potentials for metal-oxide surfaces and interfaces. *Phys. Rev. B* **50**, 11996 (1994).
56. K. Sickafus: Radiation tolerance of complex oxides. *Science* **289**, 748 (2000).
57. A. Chartier, G. Catillon, and J. Crocombette: Key role of the cation interstitial structure in the radiation resistance of pyrochlores. *Phys. Rev. Lett.* **102**, 155503 (2009).
58. R. Stoller and L. Greenwood: Subcascade formation in displacement cascade simulations: Implications for fusion reactor materials. *J. Nucl. Mater.* **271–272**, 57 (1999).
59. G. Martin, P. Garcia, L. Van Brutzel, B. Dorado, and S. Maillard: Effect of the cascade energy on defect production in uranium dioxide. *Nucl. Instrum. Methods Phys. Res., Sect. B* **269**, 1727 (2011).
60. D. Simeone, L. Luneville, and Y. Serruys: Cascade fragmentation under ion beam irradiation: A fractal approach. *Phys. Rev. E* **82**(1), 011122 (2010).
61. D. Bacorisen: Atomistic simulations of radiation-induced defect formation in spinels: $MgAl_2O_4$, $MgGa_2O_4$, and $MgIn_2O_4$. *Phys. Rev. B* **74**, 214105 (2006).
62. J. Tersoff: Carbon defects and defect reactions in silicon. *Phys. Rev. Lett.* **64**, 1757 (1990).
63. F. Gao and W. Weber: Atomic-scale simulation of 50 keV Si displacement cascades in β-SiC. *Phys. Rev. B* **63**, 054101 (2000).
64. F. Gao, W. Weber, and R. Devanathan: Atomic-scale simulation of displacement cascades and amorphization in β-SiC. *Nucl. Instrum. Methods Phys. Res., Sect. B* **180**, 176 (2001).
65. F. Gao, H. Xiao, X. Zu, M. Posselt, and W. Weber: Defect-enhanced charge transfer by ion-solid interactions in SiC using large-scale ab initio molecular dynamics simulations. *Phys. Rev. Lett.* **103**, 27405 (2009).
66. Y. Chen: *Radiation Effect and Tritium Technology for Fusion Reactor*, Vol. **2** (Gattlinburg, 1975).
67. C. Schnohr, E. Wendler, K. Gartner, W. Welsch, and K. Ellmer: Ion-beam induced effects at 15K in α-Al2O3 of different orientations. *J. Appl. Phys.* **99**, 123511 (2006).
68. W. Chu, J. Mayer, and M. Nicolet: *Backscattering Spectroscopy* (Academic Press, New York, NY, 1978).
69. B. Uberuaga: Dynamical simulations of radiation damage and defect mobility in MgO. *Phys. Rev. B* **71**, 104102 (2005).
70. F. Gao, H. Xiao, and W. Weber: Ab initio molecular dynamics simulations of low energy recoil events in ceramics. *Nucl. Instrum. Methods Phys. Res., Sect. B* **269**, 1693 (2011).
71. N. Itoh and M. Stoneham: *Materials Modification by Electronic Excitation in Insulators* (Cambridge University Press, Cambridge, UK, 2000).
72. R. Devine: Radiation induced structural changes in amorphous SiO2: 1. Point defects. *Jpn. J. Appl. Phys.* **31**, 4421 (1992).
73. N. Itoh: *Defect Processes Induced by Electronic Excitation in Insulators*, Vol. **5** (World Scientific, Singapore, 1998).
74. F. Clinard and L. Hobbs. Radiation Effects in Non-Metals In *Modern Problems in Condensed Matter Physics*, Vol. **13**, R.A. Johnson and A.N. Orlov eds.; (Amsterdam, Netherlands, 1986); pp. 387–471.
75. P. Stampfli and K. Bennemann: Theory for the instability of the diamond structure of Si, Ge, and C induced by a dense electron-hole plasma. *Phys. Rev. B* **42**, 7163 (1990).
76. K. Tanimura, T. Tanaka, and N. Itho: Creation of quasistable lattice defects by electronic excitation in SiO_2. *Phys. Rev. Lett.* **51**, 423 (1983).
77. M. Knotek and P. Feibelman: Ion desorption by core-hole auger decay. *Phys. Rev. Lett.* **40**, 964 (1978).
78. N. Itho andK. Tanimura: Formation of interstitial-vacancy pairs by electronic excitation in pure ionic crystals. *J. Phys. Chem. Solids* **51**, 717 (1990).
79. R. Williams and K. Song: The self-trapped exciton. *J. Phys. Chem. Solids* **51**, 679 (1990).
80. Y. Kayamuna: *Defects Processes Induced by Electronic Excitation in Insulators* (World Scientific, Singapor, 1989).
81. T. Tsai and D. Griscom: Experimental evidence for excitonic mechanism of defect generation in high-purity silica. *Phys. Rev. Lett.* **67**, 2517 (1991).
82. H. Hosono, H. Kawasoe, and N. Matsunami: Experimental evidence for Frenkel defect formation in amorphous SiO_2 by electronic excitation. *Phys. Rev. Lett.* **80**, 317 (1998).

https://doi.org/10.1557/jmr.2015.77 Published online by Cambridge University Press

83. G. Roma, Y. Limoge, and S. Baroni: Oxygen self-diffusion in α-quartz. *Phys. Rev. Lett.* **86**, 4564 (2001).
84. G. Xiong, A. Joly, and K. Beck, and W. hess: Laser-induced oxygen vacancy formation and diffusion on TiO_2(110) surfaces probed by photoemission electron microscopy. *Phys. Status Solidi C* **13**(10), 3598 (2006).
85. D. Stievenard, X. Boddaert, J. Bourgoin, and H. Bardeleden: Behavior of electron-irradiation-induced defects in GaAs. *Phys. Rev. B* **41**, 5271 (1990).
86. E. Seebauer and M. Kratzer: Charged point defects in semiconductors. *Mater. Sci. Eng., R* **55**, 57 (2006).
87. W. Weber, Y. Zhang, and L. Wang: Review of dynamic recovery effects on ion irradiation damage in ionic-covalent materials. *Nucl. Instrum. Methods Phys. Res., Sect. B* **277**, 1 (2012).
88. G. Krefft: Ionization-stimulated annealing effects on displacement damage in magnesium oxide. *J. Vac. Sci. Technol.* **14**, 533 (1977).
89. S. Clement and E. Hodgson: Radiation-enhanced impurity aggregation in MgO. *Phys. Rev. B* **36**, 3359 (1987).
90. R. Devanathan, K. Sickafus, W. Weber, and M. Nastasi: Effects of ionizing radiation in ceramics. *J. Nucl. Mater.* **253**, 113 (1998).
91. D. Lesueur and A. Dunlop: Damage creation via electronic excitations in metallic targets part II: A theoretical model. *Radiat. Eff. Defects Solids* **126**, 163 (1993).
92. G. Bonfiglioli, A. Ferro, and A. Mojoni: Electron microscope investigation on the nature of tracks of fission products in mica. *J. Appl. Phys.* **32**, 2499 (1961).
93. Y. Watanabe, Y. Takemoto, T. Kubozoe, and T. Mukoyama: Monte-Carlo calculations of the energy distribution of exoelectrons. *Phys. Status Solidi A* **61**, 221 (1980).
94. G. Canright: Time-dependent screening in the electron gas. *Phys. Rev. B* **38**, 1647 (1988).
95. G. Szenes: Ion-velocity-dependent track formation in yttrium iron garnet: A thermal-spike analysis. *Phys. Rev. B* **52**, 6154 (1995).
96. M. Toulemonde, C. Dufour, A. Meftah, and E. Paumier: Transient thermal processes in heavy ion irradiation of crystalline inorganic insulators. *Nucl. Instrum. Methods Phys. Res., Sect. B* **166**, 903 (2000).
97. S. Klaumunzer: Ion tracks in quartz and vitreous silica. *Nucl. Instrum. Methods Phys. Res., Sect. B* **225**, 136 (2004).
98. C. Trautmann, M. Toulemonde, K. Schwartz, J.M. Costantini, and A. Müller: Damage structure in the ionic crystal LiF irradiated with swift heavy ions. *Nucl. Instrum. Methods Phys. Res., Sect. B* **164**, 365 (2000).
99. N. Khalfaoui: Characterization of swift heavy ion tracks in CaF2 by scanning force and transmission electron microscopy. *Nucl. Instrum. Methods Phys. Res., Sect. B* **240**, 819 (2005).
100. P. Kluth: Fine structure in swift heavy ion tracks in amorphous SiO_2. *Phys. Rev. Lett.* **101**, 175503 (2008).
101. M. Backman: Atomistic simulations of MeV ion irradiation of silica. *Nucl. Instrum. Methods Phys. Res., Sect. B* **303**, 129 (2013).
102. B. Henderson and J.E. Wertz: *Defects in the Alkaline Earth Oxides* (Taylor, London).
103. T. Shen, S. Feng, M. Tang, J. Valdez, Y. Wang, and K. Sickafus: Enhanced radiation tolerance in nanocrystalline MgGa2O4. *Appl. Phys. Lett.* **90**, 263115 (2007).
104. A. Ibarra, D. Mariani, and M. Jimenez de Castro: Thermoluminescent processes of $MgAl_2O_4$ irradiated at room temperature. *Phys. Rev. B* **44**, 12158 (1991).
105. D. Simeone, G. Baldinozzi, D. Gosset, L. Mazerolles, and S. LeCaër: Impact of radiation defects on the structural stability of pure zirconia. *Phys. Rev. B* **70**, 134116 (2004).
106. D. Simeone, G. Baldinozzi, D. Gosset, S. LeCaër, and L. Mazerolles: Nano structuration of zirconia under irradiation: A way to enhance the mechanical stability of zirconia layer. *Rev. Adv. Mater. Sci.* **10**, 118 (2005).
107. S. Sorieul, T. Allard, G. Morin, B. Boizot, and G. Calas: Native and artificial radiation-induced defects in montmorillonite. An EPR study. *Phys. Chem. Miner.* **32**, 17 (2005).
108. Y. Zhang, I-T. Bae, K. Sun, C. Wang, M. Ishimaru, Z. Zhu, W. Jiang, and W.J. Weber: Damage profile and ion distribution of slow heavy ions in compounds. *J. Appl. Phys.* **105**, 104901 (2005).
109. G. Velisa, L. Thome, P. Trocellier, Y. Serruys, A. Debelle, F. Garrido, and S. Miro: Monitoring by raman spectroscopy of the damage induced in the wake of energetic ions. *J. Raman Spectrosc.* **45**(6), 481–486 (2014).
110. D. Simeone, C. Dodane-Thiriet, D. Gosset, M. Beauvy, and P. Daniel: Order–disorder phase transition induced by swift ions in $MgAl_2O_4$ and $ZnAl_2O_4$ spinels. *J. Nucl. Mater.* **300**, 151 (2002).
111. G. Guimbretière, L. Desgranges, A. Canizarès, G. Carlot, and R. Caraballo: Determination of in-depth damaged profile by Raman line scan in a pre-cut He^{2+} irradiated UO_2. *Appl. Phys. Lett.* **100**, 215914 (2012).
112. M. Ishimaru, I. AfanasyevCharkin, and K. Sickafus: Spinel-to rocksalt structural phase transformation in $MgAl_2O_4$. *Appl. Phys. Lett.* **76**, 2556 (2000).
113. G. Baldinozzi, D. Simeone, D. Gosset, S. Surble Mazerolles, and L. Thomé: Why ion irradiation does not lead to the same structural changes in normal spinels $ZnAl_2O_4$, $MgAl_2O_4$ and $MgCr_2O_4$? *Nucl. Instrum. Methods Phys. Res., Sect. B* **266**, 2848 (2008).
114. J. Cowley: *Diffraction Physics* (Amsterdam, Netherlands, 1975).
115. Y. Hirotsu, I. Afanasyev Charkin, K. Siockafus, and M. Ishimaru: Ion-beam-induced spinel-to-rocksalt structural phase transformation in $MgAl_2O_4$. *Appl. Phys. Lett.* **76**, 2556 (2000).
116. N. Nipoti: Ion implantation induced swelling in 6H-SiC. *Appl. Phys. Lett.* **70**, 3425 (1997).
117. T. Soeda and C. Kinoshita Zaluzec: Cation disordering in magnesium aluminate spinel crystals induced by electron or ion irradiation. *J. Nucl. Mater.* **283**, 952 (2000).
118. L. Luneville: Interdiffusion processes at irradiated Cr/Si interfaces. *J. Alloys Compd.* **626**, 65 (2015).
119. F. Nichols: On the estimation of sink-absorption terms in reaction-rate-theory analysis of radiation damage. *J. Nucl. Mater.* **75**, 32 (1978).
120. G. Krexner, M. Prem, F. Beneu, and P. Vajda: Nanocluster formation in electron-irradiated Li2O crystals observed by elastic diffuse neutron scattering. *Phys. Rev. Lett.* **91**(13), 135502 (2003).
121. D. Simeone, D. Gosset, J. Bechade, and A. Chevarier: Analysis of the monoclinic–tetragonal phase transition of zirconia under irradiation. *J. Nucl. Mater.* **300**, 27 (2002).
122. D. Simeone, G. Baldinozzi, D. Gosset, and J.F. Berar: Rietveld refinements performed on mesoporous ceria layers at grazing incidence. *J. Appl. Crystallogr.* **44**, 1205 (2010).
123. Y. Limoge and A. Barbu: Aging of oxides under irradiation. *Defect Diffus. Forum* **237**, 621 (2005).
124. T. Shikama and G.P. Pells: Radiation damage in pure and helium-doped α-Al_2O_3 in the HVEM qualitative aspects of void and aluminium colloid formation. *Philos. Mag. A* **47**, 369 (1983).
125. K. Yasuda, C. Kinoshita, S. Matsumura, and A.I. Ryazanov: Radiation-induced defect clusters in fully stabilized zirconia irradiated with ions and/or electrons. *J. Nucl. Mater.* **319**, 74 (2003).

https://doi.org/10.1557/jmr.2015.77 Published online by Cambridge University Press

126. A. Ryazanov, K. Yasuda, C. Kinoshita, and A.V. Klaptsov: Instability of interstitial clusters under ion and electron irradiations in ceramic materials. *J. Nucl. Mater.* **323**, 372 (2003).
127. D.G. Howitt and T.E. Mitchell: Electron irradiation damage in a-Al_2O_3. *Philos. Mag.* **44**, 229 (1981).
128. R.A. Youngman, L.W. Hobbs, and T.E. Mitchell: Radiation damage in oxides: Electron irradiation damage in MgO. *J. Phys.* **41**, C6-C227 (1980).
129. J. Soullard: Mise en evidence de boucles de dislocation imparfaites dans des echantillons de bioxyde d'uranium irradies. *J. Nucl. Mater.* **78**, 125 (1978).
130. C. Kinoshita, K. Hayashi, and S. Kitajima: Kinetics of point defects in electron irradiated MgO. *Nucl. Instrum. Methods Phys. Res., Sect. B* **1**, 209 (1984).
131. A.I. Van-Sambeek, R.S. Averback, C.P. Flynn, M.H. Yang, and W. Jäger: Radiation enhanced diffusion in MgO. *J. Appl. Phys.* **83**, 7576 (1998).
132. B. Dorado: First-principles calculation and experimental study of oxygen diffusion in uranium dioxide. *Phys. Rev. B* **83**, 035126 (2011).
133. R. Sizmann: The effect of radiation upon diffusion in metals. *J. Nucl. Mater.* **69**, 386 (1978).
134. A. Meldrum, L. Boatner, and R. Ewing: Nanocrystalline zirconia can be amorphized by ion irradiation. *Phys. Rev. Lett.* **88**, 025503 (2001).
135. R. Ewing: Ion beam induced amorphization of the pyrochlore structure type: A review. *MRS Proc.* **792**, 792-R2.1 (2003).
136. R. Belin, P. Martin, P. Valenza, and A. Scheinost: Experimental insight into based americium ceramic. *Inorg. Chem.* **48**, 5376 (2009).
137. M. Li and W. Johnson: Instability of metastable solid solutions and the crystal to glass transition. *Phys. Rev. Lett.* **70**, 1120 (1993).
138. K. Sickafus: Radiation-induced amorphization resistance and radiation tolerance in structurally related oxides. *Nat. Mater.* **6**, 227 (2007).
139. P. Gupta: Rigidity, connectivity, and glass-forming ability. *J. Am. Ceram. Soc.* **76**, 1088 (1993).
140. L. Hobbs, A. Sreeram, C. Jesurum, and B. Berger: Structural freedom, topological disorder, and the irradiation-induced amorphization of ceramic structures. *Nucl. Instrum. Methods Phys. Res., Sect. B* **116**, 18 (1996).
141. K.R. Whittle, S. Rios, K. Smith, N. Zaluzec, and G. Lumpkin: Temperature dependence of ion irradiation damage in the pyrochlores $La_2Zr_2O_7$ and $La_2Hf_2O_7$. *J. Phys.: Condens. Matter* **16**, 8557 (2004).
142. H. Xiao, W. Weber, Y. Zhang, X. Zu, and S. Li: Electronic excitation induced amorphization in titanate pyrochlore : An ab initio molecular dynamics study. *Sci. Rep.* **5**, 8265 (2015).
143. J. Gibbon: Projected range and statistic in semi conductors. *Proc. IEEE* **60**, 1062 (1972).
144. W. Weber: Models and mechanisms of irradiation-induced amorphization in ceramics. *Nucl. Instrum. Methods Phys. Res., Sect. B* **166**, 98 (2000).
145. Y. Zhang, T. Varga, M. Ishimaru, P.D. Edmondson, H. Xue, P. Liu, S. Moll, F. Namavar, C. Hardiman, S. Shannon, and W.J. Weber: Competing effects of electronics and nuclear energy loss on microstructural evolution ion ionic covalent materials. *Nucl. Instrum. Methods Phys. Res., Sect. B* **327**, 33–43 (2014).
146. M. Zheng, S. Shannon, T. Allen, D. Morgan, I. Szlufarska, and L. Jamison: Experimental and ab initio study of enhanced resistance to amorphization of nanocrystalline silicon carbide under electron irradiation. *J. Nucl. Mater.* **445**(1), 181–189 (2014).

https://doi.org/10.1557/jmr.2015.77 Published online by Cambridge University Press